Version 2013-June-10

Identification of an ancient mantle reservoir and young recycled materials in the source region of a young mantle plume: Implications for potential linkages between plume and plate tectonics

Xuan-Ce Wang[1*], Zheng-Xiang Li[1], Xian-Hua Li[2], Jie Li[3], Yi-Gang Xu[3], Xiang-Hui Li[2]

[1]*ARC Centre of Excellence for Core to Crust Fluid Systems (CCFS) and The Institute for Geoscience Research (TIGeR), Curtin University, GPO Box U1987, Perth, WA 6845, Australia*

[2]*State Key Laboratory of Lithospheric Evolution, Institute of Geology and Geophysics, Chinese Academy of Sciences, P.O. Box 9825, Beijing 100029, China*

[3]*State Key Laboratory of Isotope Geochemistry, Guangzhou Institute of Geochemistry, Chinese Academy of Sciences, Guangzhou 510640, China*

* Corresponding author. Department of Applied Geology, Curtin University, GPO Box U1987, Perth, WA 6845, Australia.

Phone:+61 8 9266 2453

Fax: +61 8 9266 3153

*E-mail: X.Wang3@curtin.edu.au

Abstract

Whether or not mantle plumes and plate subduction are genetically linked is a fundamental geoscience question that impinges on our understanding of how the Earth works. Late Cenozoic basalts in Southeast Asia are globally unique in relation to this question because they occur above a seismically detected thermal plume adjacent to deep subducted slabs. In this study, we present new Pb, Sr, Nd, and Os isotope data for the Hainan flood basalts. Together with a compilation of published results, our work shows that less contaminated basaltic samples from the synchronous basaltic eruptions in Hainan-Leizhou peninsula, the Indochina peninsula and the South China Sea seamounts share the same isotopic and geochemical characteristics. They have FOZO-like Sr, Nd, and Pb isotopic compositions (the dominant lower mantle component). These basalts have primitive Pb isotopic compositions that lie on, or very close to, 4.5- to 4.4-Ga geochrons on a $^{207}Pb/^{204}Pb$ versus $^{206}Pb/^{204}Pb$ diagram, suggesting a mantle source developed early in Earth's history (4.5–4.4 Ga). Furthermore, our detailed geochemical and Sr, Nd, Pb and Os isotopic analyses suggest the presence of 0.5–0.2 Ga recycled components in the late Cenozoic Hainan plume basalts. This implies a mantle circulation rate of >1 cm/yr, which is similar to that of previous estimates for the Hawaiian mantle plume. The identification of the ancient mantle reservoir and young recycled materials in the source region of these synchronous basalts is consistent with the seismically detected lower mantle-rooted Hainan plume that is adjacent to deep subducted slab-like seismic structures just above the core-mantle boundary. We speculate that the continued deep subduction and the presence of a dense segregated basaltic layer may have triggered the plume to rise from the thermal-chemical pile. This work therefore suggests a dynamic linkage between deep subduction and mantle plume generation.

Key words: South China Sea; basalts; ancient mantle reservoir; Hainan mantle plume; subducted oceanic crust; core-mantle boundary

1. Introduction: Plume versus plate tectonics

Subduction of oceanic slabs to as deep as the core-mantle boundary (CMB) as a part of plate tectonic processes, and the rise of hot mantle plumes from the lower mantle, are two of the first-order phenomena that operated through much of Earth's history (e.g., Hofmann and White, 1982; Li and Zhong, 2009; Zindler and Hart, 1986). However, it is still unclear how the two systems interact with each other and whether they are parts of a single geodynamic system. Answers to these questions impinge on our understanding of how the Earth works (e.g., Li and Zhong, 2009). At least some plumes are believed to have originated from the CMB, resulting in a bottom-up flux of energy and mass to the Earth's surface (e.g., Campbell and Griffiths, 1990; Griffiths and Campbell, 1990; Courtillot et al., 2003). On the other hand, high resolution seismic tomographic images (e.g., Fukao et al., 2001, 2009; van der Hilst et al., 1997) show that deep subducted slabs can penetrate the mantle transition zone, likely to fall into the lower mantle and ultimately accumulate above the CMB. It is believed that the Earth's materials are circulated between its surface and the lower mantle through these two processes.

Hofmann and White (1982) were the first to link the formation of mantle plumes to deep subduction in a conceptual model, suggesting that plumes are the results of rising long-term isolated oceanic crust at the CMB and thus a general consequence of plate tectonics. Niu and O'Hara (2003) proposed instead that plumes were produced by subducted oceanic lithospheric mantle (the harzburgite layer) at the CMB that was separated from the basaltic layer. However, because the oceanic lithospheric mantle is extremely depleted in incompatible elements, this latter model cannot explain the typical characteristics of plume-induced rocks that are enriched in incompatible elements (e.g., Hofmann, 1997; White, 2010).

Whether or not deep-subducted oceanic crust can lead to the formation of mantle plumes also depends on the balance between their thermal buoyancy and compositional buoyancy (e.g., Ogawa, 2010). Thermal buoyancy due to energy released by heat-producing elements (U, Th, and K_2O) and heat conducted from the Earth's core may ultimately overcome the negative compositional density (Ogawa, 2010; Tackley, 2011). Heat-producing element concentrations of subducted oceanic crust (Th = 0.48 ppm, U = 0.20 ppm, and K_2O = 0.33 wt.%; Stracke et al., 2003) are an order of magnitude higher than those of any peridotitic mantle reservoir including the depleted upper mantle (Workman and Hart, 2005), the chondritic bulk silicate Earth (McDonough and Sun, 1995), and the nonchondritic bulk silicate Earth (Carlson and Boyet, 2008; O'Neill and Palme, 2008). Recent numerical modelling results showed that both harzburgite and basaltic layers of subducted slabs stored at the CMB could form plume-like thermal upwelling (plumes?) or could be entrained by classic plumes (e.g., Ogawa, 2010; Tackley, 2011).

To date, geochemical, petrological, and experimental studies have recognized recycled oceanic lithospheric mantle (e.g., Lassiter and Hauri, 1998), basaltic crust (e.g., Hauri, 1996; Jackson et al., 2012; Kogiso and Hirschmann, 2006; Mallik and Dasgupta, 2012; Sobolev et al., 2000, 2005, 2007, 2011b; Takahahshi et al., 1998), gabbro (e.g., Stroncik and Devey, 2011; Yaxley and Sobolev, 2007), and sediments (e.g., Rapp et al., 2008) in mantle plumes. It is generally accepted that subducted oceanic crust and its subsequent reaction products are the dominant forms of heterogeneity in a mantle plume (e.g., Hauri, 1996; Hofmann, 1988; Hofmann, 1997; Kogiso and Hirschmann, 2006; Mallik and Dasgupta, 2012; Sobolev et al., 2000, 2005, 2007, 2011b; Takahashi et al., 1998).

Global supercontinent reconstructions and the large igneous province (LIP) record show that both the timing and location of plume events appear to have been dominantly controlled by the first order geometry of global subduction zones (e.g., Li and Zhong, 2009). It has been speculated that the sinking of subducted slabs to the lower mantle could not only push the dense chemical layer upward, but also enhance or trigger thermal instability in the lower mantle and the formation of thermal-chemical domes (and thus plumes or superplume; e.g., Li and Zhong, 2009; Steinberger and Torsvik, 2012; Zhong et al., 2007). Thermochemical convection modelling shows that the formation of the current large and isolated Pacific and African mantle superswells (or superplumes, a term we prefer to use in this paper) may be a natural consequence of such plate tectonic processes (e.g., Zhang et al., 2010; Steinberger and Torsvik, 2012). However, there are yet no clear case studies that have demonstrated the actual working of such a model with direct linkages between subduction and mantle plume formation.

The late Cenozoic basalt province in southeastern Asia (Fig. 1) is the first example that may imply direct links between a young mantle plume and deep subduction. A hypothesised young and lower mantle-rooted plume near Hainan Island is supported by the existence of extensive synchronous OIB-type basalts (e.g., Flower et al., 1992; Hoang and Flower, 1998; Tu et al., 1991; Wang et al., 2012; Zou and Fan, 2010), a lower mantle-rooted plume-like low velocity seismic structure (e.g., Huang and Zhao, 2006; Montelli et al., 2006; Zhao, 2007), a thin mantle transition zone in the region (Wang and Huang, 2012), high mantle potential temperature (Hoang and Flower, 1998; Wang et al., 2012; Wang and Huang, 2012), and geochemical signatures for the basalts suggesting a lower mantle plume origin (Zou and Fan, 2010).

On the other hand, unlike classic plumes since the Mesozoic that occur dominantly above the two mantle superplumes (e.g., Anderson, 1982; Burke and Torsvik, 2004), the Hainan plume is located within the Eurasian mantle downwelling zone and almost encircled by major subduction zones (Fig. 1). Furthermore, geophysical investigations not only identified a plume-like seismic structure (e.g., Huang and Zhao, 2006; Montelli et al., 2006; Zhao, 2007), but also detected deep-subducted slabs down to the lower mantle (e.g., Li et al., 2008a) or near the CMB (e.g., He and Wen, 2011) in this region.

The Hainan flood basalts represent a microcosm of the volcanic activity in southeast Asia (e.g., Flower et al., 1992) and are a key to unravelling the petrogenesis of the late Cenozoic basalts in this region (e.g., Wang et al., 2012; Zou and Fan, 2010). In this study, we present new high precision Pb, Sr, Nd, and Os isotope data for the Hainan flood basalts, which share the same isotopic and geochemical characteristics as synchronous basalts in the nearby Leizhou peninsula, the Indochina peninsula and the South China Sea seamounts (Fig. 1). They have FOZO-like Sr, Nd, and Pb isotopic compositions (lower mantle-origin). Their primitive Pb isotopic compositions suggest a mantle source formed early in the Earth's history (4.5–4.4 Ga). The recycled oceanic crust is likely to be very young (0.5–0.2 Ga). These new findings, along with existing geophysical, petrological, and geochemical evidence, present a strong case that a young mantle plume sampled both an ancient mantle reservoir and young recycled components.

2. Background, sampling and analytical methods

2. 1. The globally unique Hainan plume

Geophysical studies in recent years made a surprise discovery of a plume-like low-velocity structure down to the lower mantle beneath the Hainan Island-Leizhou peninsula (Leiqiong) in Southeast Asia (Fig. 1) (e.g., Huang and Zhao, 2006; Lebedev and Nolet, 2003; Lei et al., 2009; Montelli et al., 2006; Zhao, 2007), called the Hainan plume. Global seismic tomographic studies suggested that the Hainan plume is one of no more than a dozen postulated plumes of lower mantle origin worldwide (e.g., Zhao, 2007). Global occurrences of mantle plumes and subducting slabs since the Mesozoic generally feature a segregated domainal distribution, with plumes on top of the broad Pacific and African mantle superplumes and subduction in mantle downwelling zones (e.g., Li et al., 2008a; Montelli et al., 2006). However, the Hainan plume-like low-velocity structure sits close to the subduction zones of the Pacific, the Philippine Sea and the South China Sea slabs to the east, and the Indo-Australian slab to the south and west (Fig. 1), and is far away from both superplumes (e.g., Montelli et al., 2006). This makes the Hainan plume a potentially unique example amongst mantle plumes in being linked to the subduction of tectonic plates, thus shedding new insights into the workings of the global geodynamic system.

Extensive and voluminous late Cenozoic basalts are a prominent feature in southeast Asia (Fig. 1). These include continental flood basalts (CFBs) found in the Leiqiong area (called the Leiqiong CFBs) and the nearby Indochina peninsula (Fig. 1a), and seamount basalts in the South China Sea basin (Fig. 1b). The basalts have been shown to share a common source region (e.g., Hoang et al., 1996; Tu et al., 1992; Wang et al., 2012; Zhou and Mukasa, 1997). The flood basalts from the Leiqiong area and the Indochina peninsula erupted toward the end of the opening of the South China Sea between 30 and 16 Ma and lasted from about 17 Ma to younger than 1 Ma (Wang et al., 2012). Volcanic seamounts in the South China Sea have circular or oval shapes, are tens to one hundred kilometers across and thousands of meters high (Fig. 1b). Dredged basalt samples from seamounts were dated at 22–0.4 Ma (Yan et al., 2006; Yeh et al., 2010) and signify hot spot activities that may have been associated with the Hainan plume (e.g., Lebedev and Nolet, 2003; Lei et al., 2009).

The Hainan plume model is also consistent with high mantle potential temperature of 1440–1550 ^{o}C (Hoang and Flower, 1998; Wang et al., 2012), large-scale surface uplift since the late Neogene in the Indochina peninsula (Hoang and Flower, 1998) and from the Oligocene to ca. 5 Ma in southern Hainan Island (Shi et al., 2011). The identification of a hot and thin mantle transition zone also supports the lower mantle-rooted Hainan plume model – a recent seismic study demonstrated that the thickness of this mantle transition zone beneath the Leiqiong flood basalts is about 25 km thinner than the global average value, suggesting about 200 ^{o}C excess mantle potential temperature (Wang and Huang, 2012). The above evidence shows that the mantle beneath this region is ~200 ^{o}C hotter than the normal convecting upper mantle (e.g., Herzberg et al., 2007; Lee et al., 2009).

The synchronous late Cenozoic basalts in the Leiqiong area, the Indochina peninsula, and the South China Sea seamounts display light rare earth element (LREE) enriched patterns, typical ocean island basalt (OIB)-type incompatible element distributions, normal OIB-like Sr and Nd isotopic compositions, and Dupal-like EM2 (enriched mantle 2) Pb isotope signatures (e.g., Han et al., 2009; Hoang et al., 1996; Tu et al., 1991, 1992). Recent studies proposed that the Dupal-like EM2 isotopic signature may have originated from partial melting of lower mantle materials entrained in the rising Hainan plume (e.g., Zou and Fan, 2010).

2.2. Regional geology and sampling

Twenty-seven fresh basalt samples were collected from the north of Hainan Island for Nd-Pb isotopic analysis, with 24 of these further analysed for Sr isotopes, and 17 for Re and Os concentrations and Os isotopic ratios. All the samples have been previously analysed for petrography, major-trace element compositions, and for $^{39}Ar/^{40}Ar$ ages (Wang et al., 2012). Chips of the samples were washed ultrasonically in double-deionized water and then hand-picked under a binocular microscope to avoid any alteration and/or fractured surfaces. They were crushed to fine powders. The results are presented in Appendix Tables S1 and S2 and Figures 2–5.

2.3. Analytical methods

For lead isotopic analyses, 100-150 mg of each whole rock powder was dissolved with distilled HF+HNO_3 in Savillex Teflon screw-cap beakers at 150 °C for seven days. Lead was separated and purified using anion resin exchange techniques with HBr as eluant. Procedural blanks were < 0.2 ng for Pb. Isotopic ratios were measured on a Finnigan MAT-262 thermal ionization mass spectrometer (TIMS) at the Institute of Geology and Geophysics, Chinese Academy of Sciences, Beijing. Lead was loaded with a mixture of Si-gel and H_3PO_4 onto a single-Re filament and measured at 1300°C. Measured Pb isotopic ratios were corrected for instrumental mass fractionation of 0.11% per atomic mass unit by reference to repeated analyses of the NBS-981 Pb standard. Repeated analyses of NBS-981 gave $^{204}Pb/^{206}Pb = 0.05897 \pm 0.00015$, $^{207}Pb/^{206}Pb = 0.91445 \pm 0.00080$, $^{208}Pb/^{206}Pb = 2.1617 \pm 0.0018$ (2σ).

Rhenium-Osmium isotopes of the samples were determined at the Guangzhou Institute of Geochemistry. Powdered bulk rock samples (2–3g each) were spiked with solutions enriched in ^{190}Os and ^{185}Re and digested in inverse aqua regia in a sealed

Carius tubes at 240°C for at least 24 hours (Shirey and Walker, 1995). Osmium was extracted by carbon tetrachloride and subsequently back extracted into high-purity concentrated HBr (Pearson and Woodland, 2000). Further purification of Os was accomplished via microdistillation in a conical Teflon vial. Afterwards, Re was extracted from the solution in anion exchange columns (AG1×8, 200–400 resin). Os isotope measurements were conducted by negative thermal ionization mass spectrometer (N-TIMS) on a Thermo-Fisher TRITON instrument (Creaser et al., 1991). Total blank levels were 3.0±0.9 pg and 10.6±0.5 for Os and, Re (2 SD, n = 6), respectively. Both Os and Re were corrected for blanks. The blank $^{187}Os/^{188}Os$ ratio was 0.256 ± 0.034 (2 SD, n = 6). The quality of the Os data was also confirmed in a comparative analytical study using the international peridotite standard rock WPR-1. During the course of this study, WPR-1 yielded $^{187}Os/^{188}Os$ ratio of 0.14475 ± 0.00057 (2 SD, n = 6), and the Re and Os concentrations (ppb) were 10.7 ± 0.6 and 17 ± 1 (2 SD, n = 6) for five measurements, respectively.

Neodymium isotopic compositions were determined using a Micromass Isoprobe multi-collector ICP-MS (MC-ICP-MS) at the Guangzhou Institute of Geochemistry, following analytical procedures described in Li et al. (2004). Measured $^{143}Nd/^{144}Nd$ ratios were normalized to $^{146}Nd/^{144}Nd$ = 0.7219, and the reported $^{143}Nd/^{144}Nd$ ratios were further adjusted relative to the Shin Etsu JNdi-1 standard of 0.512115, corresponding to the La Jolla standard of 0.511860 (Tanaka et al., 2000). During the course of this study, international standard rocks BHVO-2, JB-1 and JB-3 yielded $^{143}Nd/^{144}Nd$ = 0.512970 ± 8 (2σ, n = 5), 0.512778 ± 5 (2σ, n = 5), 0.513063 ± 13 (2σ, n = 4), respectively.

3. Results

3.1 Sr-Nd-Pb isotopes

The Sr-Nd-Pb isotope data are presented in Appendix Table S1 and Figures 2 and 3. The Hainan basalts exhibit fairly uniform $^{87}Sr/^{86}S$ (0.7045–0.7031) and $^{143}Nd/^{144}Nd$ (0.51287–0.51297) ratios, with average values of 0.7039 ± 0.0005 (1 SD) and 0.51287 ± 0.00005 (1 SD), respectively. This is comparable to the present-day value for the superchondritic Earth model (SCHEM, a nonchondritic bulk silicate Earth) with $^{143}Nd/^{144}Nd$ = 0.512997 ± 0.000103 and $^{87}Sr/^{86}S$ = 0.7030 ± 0.004) (Caro and Bourdon, 2010). The oceanic basalt-like Nb/U ratios, the broad negative correlation between MgO/SiO_2 and εNd, and the lack of correlation between Nb/U and εNd rule out significant crustal contamination in the generation of the Hainan basalts (Fig. 2). The studied samples display a narrow range of $^{206}Pb/^{204}Pb$ ratios (18.6–18.8), but a relatively large rang of $^{207}Pb/^{204}Pb$ (15.45–15.65) and high $^{208}Pb/^{206}Pb$ ratios (38.4–39.1). They define a good linear correlation of ($^{207}Pb/^{204}Pb$) = 0.4567 (± 0.0791) × ($^{206}Pb/^{204}Pb$) + 7.0702 (±1.4717), r = 0.76 (Fig. 3a). This linear correlation, when interpreted as a model isochron, yielded an source differentiation age of 4.1 ± 0.3 Ga, which is much older than those of global oceanic basalts at 2.0 ± 0.2 Ga (e.g., Sun, 1980). This implies long-term isolation of the Hainan mantle source from the Earth's mantle stirring (e.g., Allegre and Lewin, 1995), and possibly formed in Earth's early history (e.g., Jackson et al., 2010). Another prominent characteristic of the studied Hainan samples is linear correlation between εNd and $^{208}Pb^*/^{206}Pb^*$[$^{208}Pb^*/^{206}Pb^*$ = ($^{208}Pb/^{204}Pb$ - 29.475)/($^{206}Pb/^{204}Pb$ - 9.306) (Hofmann, 1997)] (red filled circles in Fig. 3d). This means that Th/U correlate with Sm/Nd in the Hainan mantle plume evolution.

Figure 3 also shows that the Pb, Sr, and Nd isotopic compositions of the studied samples are comparable to those of young Indian-Ocean MORBs, and show an affinity with the FOZO (focal zone) mantle component.

3.2 Re-Os isotopes

The Re-Os concentration and isotopic results are given in Appendix Table S2 and Figures 4 and 5. Osmium concentrations range from 0.009 to 10.87 ppb (mostly 0.1 to 0.4 ppb) and rhenium concentrations vary from 0.027 to 0.199 ppb. $^{187}Re/^{188}Os$ ratios range from 0.088 to 21 (mostly 1.1 to 5.3). $^{187}Os/^{188}Os$ ratios range from 0.1227 to 0.1829 (mostly 0.129 to 0.150). The osmium concentrations of the Hainan basalts plot in the fields of normal OIB and high-magnesium lavas (Fig. 4a), being significantly higher than most MORBs (mostly <0.05 ppb) (e.g., Gannoun et al., 2007; Schiano et al., 1997; Shirey and Walker, 1998) and synchronous (3–17 Ma) Philippine Sea plate seamount basalts of nonplume origin (mostly <0.07 ppb; Dale et al., 2008). The Hainan basalts have low Re contents compared with those of MORB. The Os isotopic ratios of the Hainan basalts (Os $\geq$ 0.07 ppb) are similar to those of the Hawaiian plume-originated OIBs and early Iceland plume-related high-magnesium lavas (Fig. 4b).

There are covariations of $^{187}Os/^{188}Os$ with Os concentration and $^{187}Re/^{188}Os$ ratios in the Hainan flood basalts (Fig. 4b and c). Sample 08HN-22D possesses the highest Os concentration (10.87 ppb) and the lowest $^{187}Os/^{188}Os$ ratio (0.1227). In contrast, 08HN-5F and 08HN-14A have the lowest Os concentrations (0.025 and 0.009 ppb, respectively) and the highest $^{187}Os/^{188}Os$ ratios. Excluding the end-member samples, there are no meaningful correlations of $^{187}Os/^{188}Os$ with Os and $^{187}Re/^{188}Os$. With the exception of sample 08HN-5F, the Hainan basalts define a good correlation between $^{187}Os/^{188}Os$ and Fe/Mn (Fig. 4d).

4. Discussion

4.1 Contamination versus source heterogeneity

Our new isotope data, along with a compilation of published data from the Hainan Island-Leizhou peninsula (the Leiqiong area) (Flower et al., 1992; Han et al., 2009; Tu et al., 1991; Wang et al., 2012; Zou and Fan, 2010), the Indochina peninsula (Hoang et al., 1996; Zhou and Mukasa, 1997) and the South China Sea seamount basalts (Tu et al., 1992; Yan et al., 2008), are plotted in Figures 2 and 3.

As shown in Figure 2a, the high-εNd (> +3) samples define a broad negative correlation between εNd and MgO/SiO_2, whereas the low-εNd (≤+3) samples, mostly from the Indochina peninsula, have a positive correlation. The oceanic basalt-like Nb/U ratios and the correlation between Nb/U and εNd (Fig. 2b) further demonstrated that the effect of crust contamination is insignificant in high-εNd (> +3), but the low-εNd (≤ +3) samples underwent significant crustal contamination. Such samples will be excluded from further discussions.

Within the 17 analyses, sample 08HN-22D represents an Os-rich and ^{187}Os-depleted end-member, a typical characteristic of sub-continental lithospheric mantle (SCLM)-derived melts (Figs. 4 and 5). Because the partial melting mainly occurred within the asthenospheric mantle (Wang et al., 2012), the Hainan basalts may have been affected by assimilation of SCLM. The Os concentration of sample 08HN-22D is higher than both fertile (2.8–3.4 ppb) and depleted mantles (0.8–9 ppb) and komatiites (0.5–6 ppb) (Shirey and Walker, 1998). Such an extreme enrichment of Os requires a very high proportional involvement of SCLM. This is inconsistent with its incompatible trace element and Sr-Nd isotope compositions. It has OIB-like trace element compositions, such as high Nb/La (1.34), La/Sm (5.8) and Re (0.199 ppb) and low Sm/Nd (0.19). In addition, this sample has Sr ($^{87}Sr/^{86}Sr$ = 0.7041) and Nd (εNd = +4.2) isotopes similar to the other 16 samples (Figs. 3 and 4). These features therefore suggest the involvement of trace Os-enriched phases (e.g., Os-bearing sulfides or Os alloy phases) through assimilation or entrapment. Such trace phases, probably originating from within the SCLM, would have caused the Os-rich and ^{187}Os-depelted features of the primary melt, but have had little effect on incompatible trace element concentrations (such as Re) and Sr-Nd isotopic ratios due to mass balance.

Samples 08HN-14A and 08HN-5F represent the Os-poor and ^{187}Os-enriched end-member (Figs. 4 and 5). This characteristic can be attributed to assimilation of continental crust or injection of recycled oceanic crust into the source region. Incompatible trace element signatures of continental crust and recycled oceanic crust are different (Fig. 5a and b). For example, the oceanic crust is characterized by high Sm/Nd (0.28–0.38) and low La/Sm (0.74–1.85; Stracke et al., 2003), whereas continental crust displays low Sm/Nd (0.17–0.25) and high La/Sm (2.9–6.6; Rudnick and Gao, 2003). Thus, the mixing of continental or oceanic crust with asthenospheric mantle-derived melts would produce different trends (Fig. 5a and b). As shown in Figures 5a and b, with the exceptions of the two end-members (08HN-22D and 08HN-14A), the remaining samples define good linear correlations of Os with Sm/Nd and La/Sm. The Os-poor ends of each linear trend converge to recycled oceanic crust rather than to continental crust (Fig. 5a and b). This is inconsistent with crustal contamination. Compared with the main linear trends, sample 08HN-14A is characterized by its depletion in Os at given Sm/Nd and La/Sm ratios (Fig. 5a and b). This may have been caused by either crustal contamination or the loss of sulphides. The characteristics of high Nb/La ratio (1.5), high εNd value (+5.7) and low $^{87}Sr/^{86}Sr$ (0.703) ratio of this sample exclude the possibility that the depletion in Os was a result of crustal contamination. Thus, the decoupling of Os is likely attributed to loss in sulphides that co-precipitated with silicate. The large ranges in Os concentration and $^{187}Os/^{188}Os$ ratio are therefore attributed mainly to mantle source heterogeneity rather than crustal contamination.

4. 2 Lower mantle isotopic characteristics

The synchronous less-contaminated basalts (εNd>+3) from the Leiqiong area, the Indochina peninsula, and the South China Sea seamounts (called the LIS basalts hereafter) share common Sr-Nd-Pb isotopic characteristics (Figs. 2 and 3). They fall close to or within the range suggested for a FOZO (focal zone) mantle component (Hauri et al., 1994). FOZO is commonly identified as a major component of the lower mantle (e.g., Campbell and O'Neill, 2012; Hart et al., 1992; Hauri et al., 1994).

The osmium isotopic ratios and Re and Os concentrations of the Hainan basalts (Os ≥ 0.07 ppb) are similar to those of lower mantle-rooted plume-induced basalts, such as the Hawaiian plume OIBs and the ca. 60 Ma Iceland plume picrites (Fig. 4), suggesting a lower mantle origin.

The lower mantle Sr, Nd, Pb, and Os isotopic signatures are therefore consistent with the previously proposed lower mantle-rooted Hainan plume model (e.g., Huang and Zhao, 2006; Montelli et al., 2006; Wang et al., 2012; Zhao, 2007; Zou and Fan, 2010). The low-temperature thermochronological evidence for a 30–23 Ma episode of rapid uplift and unroofing in Hainan Island (Shi et al., 2011), early (about 22 Ma) hot spot activity (Fig. 1b), and possible ca. 30 Ma plume-induced magmatic events (e.g., Yeh et al., 2010) imply that the head of the Hainan plume likely impinged on the base of the lithosphere at around 30 Ma.

4. 3. A very early-formed mantle reservoir for the Hainan plume

The LIS basalts are characterized by a narrow range of $^{206}Pb/^{204}Pb$, but large variations in $^{207}Pb/^{204}Pb$, leaving them well bracketed by the 4.5 and 4.4 Ga geochrons (Fig. 3a). Such a Pb isotopic characteristic suggests that these basalts were derived mainly from an early Earth mantle reservoir that has remained in isolation since the earliest days of planetary accretion some 4.5 Ga ago (e.g., Jackson and Carlson, 2011; Jackson et al., 2010).

If the composition of such an ancient mantle reservoir either represents that of the bulk silicate Earth (Andreasen et al., 2008) or was formed shortly after the formation of the core and has remained unaffected by subsequent events, then the εNd [$\varepsilon Nd = [(^{143}Nd/^{144}Nd)_{sample}/0.512638-1] \times 10{,}000$] value for the ancient reservoir today should be +5 to +9 (e.g., Bourdon et al., 2008; Caro and Bourdon, 2010). The less-contaminated LIS basalts have εNd values ranging from about +3 to +8 (Figs. 2 and 3), similar to the present-day value predicted for the ancient mantle reservoir. Similar Nd isotopic characteristics have also been recognized in other plume-related flood basalts (Jackson and Carlson, 2011) and in two oceanic plateaus—the Kerguelen and Ontong Java plateaus (Campbell and Griffiths, 1992; Campbell and O'Neill, 2012). The ancient mantle reservoir components plot within 100 Ma of the 4.5-Ga geochron on a $^{207}Pb/^{204}Pb$ versus $^{206}Pb/^{204}Pb$ diagram, suggesting that they were developed early in Earth's history (e.g., Jackson and Carlson, 2011).

Previous studies (Jackson and Carlson, 2011; Jackson et al., 2010) suggested that such an ancient mantle reservoir represents a residue of an ancient global depletion event. However, the estimated Nb/La ratios for such an ancient reservoir is 1.41 (Jackson et al., 2010) that is much higher than any known depleted reservoir, such as the modern depleted mid-ocean-ridge basalt (MORB) mantle reservoirs (Nb/La = 0.64–0.97; Workman and Hart, 2005) and the early depleted reservoirs (Nb/La = 0.74–0.79; Carlson and Boyet, 2008). Furthermore, this implies that such an ancient reservoir is rather enriched in terms of the Nb/La ratio. This study shows that this ancient mantle reservoir also has a large range of $^{208}Pb^*/^{206}Pb^*$ values (Fig. 3d) and high $^{208}Pb^*/^{206}Pb^*$ values similar to some EM-1 type OIBs (e.g., Hofmann, 1997). This suggests an enriched component with Th/U ratios >4. The high end-member of the $^{208}Pb^*/^{206}Pb^*$ array is associated with the lowest εNd values (about +3.5), again suggesting an enriched end-member. Thus, the ancient mantle reservoir is likely chemically heterogeneous, possibly containing both depleted (low-$^{208}Pb^*/^{206}Pb^*$ and high- εNd) and enriched (high-$^{208}Pb^*/^{206}Pb^*$ and low-εNd) end-member components.

To understand the formation of such an ancient mantle reservoir requires knowledge about the density contrast between solid and melt fractions (e.g., Lee et al., 2010; Nomura et al., 2011). The prevailing view is that the differentiation of Earth's silicate mantle was driven by the extraction of low-density melts. Lee et al. (2010) proposed a fresh perspective on the way of silicate differentiation occurred in the early Earth whereby liquids sink instead of rising. It was suggested that under certain high-pressure conditions in the upper mantle, peridotite partial melts may be more dense than solid peridotite because such liquids are Fe-rich and more compressible than solids (e.g., Lee et al., 2010; Miller et al., 1991; Stolper et al., 1981; Suzuki et al., 1998). Recent experimentally determined iron partitioning over the entire mantle pressure range also suggests that liquids formed at ≥1,800 km are denser than coexisting solids in the lower mantle (Nomura et al., 2011).

Crystallization of a magma ocean would produce an enriched denser liquid phase at ≥1,800 km (e.g., Caro et al., 2005; Labrosse et al., 2007; Nomura et al., 2011). Shortly after magma ocean crystallization, a high degree of partial melting of depleted peridotite at depth of 300-410 km depths (Lee et al., 2010) would produce depleted type of denser melt. Thus, early global differentiation of bulk silicate Earth at 4.55–4.40 Ga might have resulted in both enriched and depleted types of denser melts that were preserved close to the CMB (Jackson and Carlson, 2011; Lee et al., 2010; Nomura et al., 2011), isolated from subsequent mantle convection (Carlson and Boyet, 2008; Coltice et al., 2011; Nomura et al., 2011).

4. 4 A minor 0.5–0.2 Ga recycled component in the source region of the Hainan plume

Our new Os isotopic results suggest high- and low-Os end-members for the generation of the Hainan basalts (Fig. 5). The high-Os end-member displays typical characteristics of a melt generated from a peridotitic source, such as low SiO_2 and Sm/Nd and high MgO, La/Sm and Os (≥0.4 ppb). In contrast, the low-Os end-member shows an affinity to melts derived from pyroxenitic sources with high silica and Sm/Nd and low MgO and La/Sm (Fig. 5 and Appendix Fig. S1). The studied samples display moderate correlations of $^{187}Os/^{188}Os$ with SiO_2 (r = 0.53, Appendix Fig.S1c) and MgO (r = -0.63, Appendix Fig. S1d), and a good correlation with Fe/Mn (r = 0.90), also evidence for the presence of pyroxenitic components in the source region.

The Os characteristics of our samples are consistent with previous findings that the source of the Hainan basalts is a mixture of predominantly mantle peridotite with some mafic components (Wang et al., 2012). The mafic components were likely derived from recycled oceanic crust, as suggested by the high Fe/Mn ratios, high Ni contents and positive Sr anomalies (Wang et al., 2012) and Os isotopes (this study).

The LIS basalts are also characterized by evolution from high- and low-silica end-member melts (Wang et al., 2012; Fig. 6). The high-silica end-member is characterized by depletions in incompatible trace elements, low Os, K_2O, TiO_2 and MgO, and high Fe/Mn and $^{187}Os/^{188}Os$ (Wang et al., 2012; this study). As shown in Fig. 6, the high-silica end-member is similar to melt derived from bulk recycled oceanic crust (ROC; Stracke et al., 2003) and oceanic gabbro (Yaxley and Sobolev, 2007). By contrast, the low-silica end-member has 44 wt.% SiO_2, 2.5 wt.% TiO_2 and 18 wt.% MgO (Wang et al., 2012), which compares well with the composition of partial melt of garnet peridotite at 3 GPa and 1430–1460 ^{o}C (Davis et al., 2011).

The isotopic composition of recycled components is strongly dependent on parent-daughter ratios and recycling ages (e.g., Sobolev et al., 2011a; Stracke et al., 2003, 2005). Recycling time estimations for subducted oceanic crust vary from 1–2.5 Ga (e.g., Allegre and Lewin, 1995; Sun, 1980) to 0.2–1.0 Ga (e.g., Becker, 2000; Sobolev et al., 2011a). Therefore, young and ancient recycled components should possess unique time-integrated isotope signatures (e.g., Demény et al., 2004; Stracke et al., 2003, 2005). As a consequence, mixing between typical mantle peridotite and ancient recycled oceanic crust can produce correlations between isotopic ratios and major elements (e.g., Hauri, 1996; Huang and Frey, 2005; Jackson et al., 2012; Kokfelt et al., 2006), and/or trace element ratios (e.g., Demény et al., 2004; Kokfelt et al., 2006; Lassiter and Hauri, 1998).On the contrary, injection of recent recycled oceanic crust into peridotitic source should produce good correlations between major and trace elements, but good correlations between isotopes and elements are not expected. The latter has been observed in the LIS basalts (Fig. 6 and Appendix Figs. S1 and S2), suggesting a young recycled component in their source. This is illustrated by the following numerical modelling of isotope evolution.

The initial Sr, Nd and Pb isotope composition of ancient oceanic crust at the time of recycling is modeled according to the method proposed by Stracke et al. (2003) with changes made to some parameters. Because the averages of global MORB and south Indian Ocean MORB plot on the 4.45-Ga and 4.48-Ga geochrons, the differentiation age at which time the MORB mantle was derived from the bulk silicate Earth is adjusted from 2.0 Ga (Stracke et al., 2003) to 4.5 Ga. Due to homogeneous and superchondritic $^{142}Nd/^{144}Nd$ isotopic ratios in all modern terrestrial samples (e.g., Jackson and Carlson, 2012), our calculation was undertaken using a super-chondritic Earth Model (SCHEM) (Caro and Bourdon, 2010) following a two-stage evolutionary model (Stracke et al., 2003). Because the average Sr and Nd isotopes of south Indian Ocean MORB, with $^{143}Nd/^{144}Nd = 0.5130 \pm 0.0001$ (1 SD, n = 292) and $^{87}Sr/^{86}Sr = 0.7031 \pm 0.0004$ (1 SD, n = 255), are identical to those of SCHEM whose average Pb isotope plots on the 4.5-Ga geochron, the average Pb isotopes of the south Indian Ocean MORB were used to calculate the initial Pb isotope of recycled oceanic crust with $\mu = {}^{238}U/^{204}Pb = 8.7$, $^{232}Th/^{238}U = 3.8$. A quantitative Os isotopic modelling method (Dale et al., 2007) has also been applied to test the effect of lithologies and recycling ages on the range of Pb-Os isotopes of the recycled components (Fig. 7).

The modelling results (Figs. 3 and 7) have several important implications. First, the present-day Pb isotopic compositions of recycled components evolved along the OIB arrays as a function of recycled ages (Fig. 3a and b). This implies that recycled oceanic crust may be the dominant factor controlling Pb isotopic heterogeneities in OIB sources. The lead isotopic array of $^{206}Pb/^{204}Pb$-$^{207}Pb/^{204}Pb$ implies that the age of recycled oceanic crust should be younger than 0.6 Ga (Fig. 3a) in the source of LIS basalts. Second, extremely high $^{187}Re/^{188}Os$ ratios recently reported in oceanic crust (80 to 675) (e.g., Dale et al., 2007; Peucker-Ehrenbrink et al., 2012) would lead to extremely radiogenic $^{187}Os/^{188}Os$ ratios ($^{187}Os/^{188}Os$ = 2– 12) over 1 Ga (Fig. 7a), suggesting that such a component cannot be present in the LIS basalt source. Third, both ancient (> 0.6 Ga) gabbro- and bulk oceanic crust-derived melts possesses distinctive Pb-Sr-Nd (Fig. 3) and Os (Fig. 7) isotopic signatures that are significantly different from what we observe in the LIS basalts. Overall, our modelling suggests that the age of recycled oceanic crust in the LIS mantle source should be younger than 0.6 Ga, probably 0.5– 0.2 Ga. Such a young age is comparable with the age range of 0.65– 0.20 Ga for recycled oceanic crust in the source region of the Hawaiian OIBs (Sobolev et al., 2011a).

Although the current data support the recycled oceanic crust model, the following evidence shows that it was only a minor component in the mantle source region. Figure 6a shows that the La/Sm-Sm/Nd array of the LIS basalts matches well with partial melting of a peridotitic source. This implies that partial melting processes may be a controlling factor for the geochemical diversity. Variations in major element compositions may also be attributed to partial melting processes (Fig. 6b). Furthermore, the inferred residual mineral assemblages indicate that the source of the high-silica melts (tholeiites) should be dominantly peridotite (Wang et al., 2012). In addition, we demonstrated above that the low-silica end-member melts were derived mainly from peridotitic sources. We thus conclude that the $^{207}Pb/^{204}Pb$–$^{206}Pb/^{204}Pb$

array in Figure 3a should be mainly attributed to an ancient peridotitic source, and this suggests an early isolation of the FOZO-like component.

4. 5. Possible linkage between mantle plume and plate tectonics

The unique tectonic setting for the Hainan plume implies that it may be genetically linked to the sinking of subducted slabs surrounding it to the core-mantle boundary. Geophysical studies identified stagnated oceanic slabs at both the mantle transition zone in the vicinity of Hainan Island and ongoing subduction reaching the lower mantle (e.g., He and Wen, 2011; Huang and Zhao, 2006; Huang et al., 2010; Li et al., 2008a; Zhao, 2004; Zhao et al., 2011). High-quality differential-travel-time analysis further revealed that the lower mantle beneath the South China Sea has a weak low velocity anomaly that is nearly encircled by two prominent high velocity patches above the CMB (He and Wen, 2011). The two high velocity anomalies have been interpreted as representing subducted Pacific and Indo-Australia plates in the past 30–60 Ma (He and Wen, 2011). Based on the seismic, geochemical and geological evidence, we propose that the avalanches of the subducted Indo-Australian and Pacific slabs to the core-mantle boundary may have pushed up a thermal-chemical pile to form the Hainan plume (Fig. 8 and detailed discussion below) following conceptual models by Maruyama (1994) and Li et al. (2008b).

High-resolution seismic images (Lei et al., 2009) show a bent geometry of the Hainan plume in the upper mantle, which may be attributed to shallow mantle circulation (Lei et al., 2009). The presence of both a large scale (1000-2000 km wide) and thin low-velocity layer under the South China Sea below the 660-km discontinuity (e.g., Zhao, 2007) and a small-scale thin mantle transition zone with a diameter of about 200 km beneath northwest Hainan Island may reflect the ponding of hot plume materials beneath the transition zone (e.g., Lei et al., 2009; Wang and Huang, 2012). A similar broad seismic structure has been found beneath the transition zone west of Hawaii (Cao et al., 2011), suggesting that the typical plume-induced Hawaiian volcanism may not have been caused by a stationary narrow plume that rose from the CMB, but by hot plume materials first held back beneath the 660 km discontinuity, and then entrained under the transition zone before rising up to the surface (Cao et al., 2011). However, the Hainan plume may be more complex than the Hawaii plume because of the influence of deep subduction (Lei et al., 2009). Interactions between the mantle plume, the mantle transition zone, stagnant slabs, and previous mid-ocean ridges may have transformed the lower mantle plume into several smaller secondary thermal upwellings in the upper mantle (Cao et al., 2011; Davies and Bunge, 2006) (Fig. 8).

The presence of 0.2–0.65 Ga (Sobolev et al., 2011a) and 0.5–0.2 Ga young recycled sources in the Hawaiian and Hainan plumes, respectively, imply a timescale of general mantle circulation with a rate higher than 1 cm/yr, assuming that subducted crust was delivered to the CMB at 2,900 km depth, and the Hawaiian and Hainan plumes rise from that depth. However, strong ^{230}Th excesses suggest a slow upwelling rate (<1cm/yr) for the Hainan plume (Zou and Fan, 2010). The difference can be reconciled because the U-series data reflect recent (< 0.35 Ma) upwelling rates whereas this study provides an average long-term upwelling rate.

5. Conclusions

In this study, we present new high precision Pb, Sr, Nd, and Os isotope data for the Hainan flood basalts. Together with a compilation of published data, our work shows that less contaminated and synchronous basaltic samples from the Hainan-Leizhou peninsula, the Indochina peninsula and the South China Sea seamounts have FOZO-like Sr, Nd, and Pb isotopic compositions. Their primitive Pb isotopic compositions suggest a mantle source developed early in the Earth's history (4.5–4.4 Ga). A very young (0.5–0.2 Ga), but minor, recycled component is also suggested to have contributed to the Hainan plume basalts. The presence of a 0.5–0.2 Ga recycled component in the late Cenozoic basalts suggests a mantle circulation at a rate higher than 1 cm/yr. The identification both of an ancient mantle reservoir and young recycled materials in the young Hainan plume is consistent with geophysical observations showing a plume adjacent to deep subducted slab-like seismic structures just above the core-mantle boundary. We therefore propose a dynamic linkage between deep subduction and mantle plume generation.

Acknowledgements

We thank reviewers Albrecht W. Hofmann and Hai-Bo Zou, and editor T. Mark Harrison for their constructive and helpful reviews. We are grateful to W.G. Long, J.B. Zhou, and Y.H. Ling (Hainan Institute of Geological Survey, Haikou, China) for help with the fieldwork; C.F. Li and Q.L. Li (State Key Laboratory of Lithospheric Evolution, Institute of Geology and Geophysics, Chinese Academy of Sciences) for the isotopic analyses; and S.A.Wilde (Curtin University) for constructive suggestions and proofreading. This work was supported by the National Science Foundation of China (grants 41173038, 40803010, and 40973044), the CAS/SAFEA International Partnership Program for Creative Research Teams (KZCX2-YW-Q04-06), ARC Discovery Project grant (DP110104799), and an ARC DECRA Fellowship through the ARC Centre of Excellence for Core to Crust Fluid Systems (CCFS). This is TIGeR publication No. 474 and CCFS contribution xxx.

Figure Captions

Fig. 1 Geological and bathymetric map of the South China Sea and adjacent regions showing late Cenozoic basaltic volcanism, ridge spreading directions and seamounts in the South China Sea (SCS). Italic numbers in white in (**a**) show the spreading ages in Ma (Braitenberg et al., 2006). Inset in (**a**) shows the major subduction zones in the region where HI stands for Hainan Island. (**b**) Three-dimensional geomorphologic features of seamounts in the South China Sea modified after Braitenberg et al. (2006). Yellow stars are sites where seamount basalts have been dated (Yan et al., 2006). The bathymetric map in (**a**) is from website: http://cmtt.tori.org.tw/data/Appmap/maplist.htm.

Fig. 2 Plots of (a) MgO/SiO_2 and (b) Nb/U against εNd values for late Cenozoic basalts from the Leiqiong area (Flower et al., 1992; Han et al., 2009; Tu et al., 1991; Wang et al., 2012; Zou and Fan, 2010), the Indochina peninsula (Hoang et al., 1996; Zhou and Mukasa, 1997) and the South China Sea seamount (Tu et al., 1992; Yan et al., 2008). $\varepsilon Nd(t) = [(^{143}Nd/^{144}Nd)_{sample}/0.512638-1] \times 10{,}000$. The corresponding major-trace element data for the Hainan basalts analysed in this study are from Wang et al. (2012). Nb/U is one of the most effective parameter for discriminating between crustal and mantle-derived materials (e.g., Hofmann, 1997; Hofmann et al., 1986). Basalts from the Leiqiong area and the South China Sea seamounts have Nb/U ratios similar to those of oceanic basalts (37–57; Hofmann et al., 1986) with little correlation with εNd, indicating insignificant crustal contamination. By contrast, the high-εNd (> +3) samples from the Indochina peninsula have high Nb/U ratios, varying from ~40 to 70 and negatively correlated with εNd, whereas the low-εNd (≤ +3) samples from the same region have lower Nb/U ratios similar to those of continental crust (10;

Hofmann et al., 1986) and positively correlated with εNd. These diagrams show that the samples with εNd ≤ +3 are significantly affected by crustal contamination. The Nb/U values for oceanic basalts and continental crust are from Hofmann et al. (1986).

Fig. 3 Sr, Nd and Pb isotopes of least-contaminated late Cenozoic LIS basalts from the Leiqiong area, the Indochina peninsula, and the South China Sea seamounts compared with the Pacific and south Indian Ocean MORBs. The fields of the Pacific and south Indian Ocean MORBs were based on data compilation by Meyzen et al. (2007). The field of FOZO (focal zone) mantle component is defined by $^{87}Sr/^{86}Sr$ = 0.703–0.704, $^{143}Nd/^{144}Nd$ = 0.5128–0.5130, $^{206}Pb/^{204}Pb$ = 18.5–19.5, $^{207}Pb/^{204}Pb$ = 15.55–15.65, $^{208}Pb/^{204}Pb$ = 38.8–39.3, and $^{208}Pb^{*}/^{204}Pb^{*}$ = 0.964– 1.014 (Hauri et al., 1994). The isotope evolution of recycled oceanic crust (99% bulk igneous crust + 1% sediments), bulk recycled igneous crust (25%N-MORB + 25% altered MORB + 50% gabbro), and gabbros are shown. Numbers next to crosses indicate the recycling ages (in Ga). To minimize the effect of crustal contamination, samples with εNd ≤+3 have been excluded. Data sources are the same as for Figure 2. OIB arrays: $^{207}Pb/^{204}Pb$–$^{206}Pb/^{204}Pb$ OIB array, y = 13.605 + 0.1025x (r = 0.88, n = 660); $^{208}Pb/^{204}Pb$–$^{206}Pb/^{204}Pb$ OIB array, y = 22.321 + 0.871x (r = 0.90, n = 660). OIB lead isotopic data used in linear regression are from the Georoc database (georoc.mpchmainz.gwdg.de/georoc). Only OIB samples with SiO_2 = 44–51 wt.%, MgO = 10–18 wt.%, and totally dry between 97 wt.% to 101 wt.% were used. The parent-daughter ratios used for the calculation have taken into account the effect of subduction processes (e.g., Stracke et al., 2003). See text for details about calculation of initial isotopic compositions. Other related parameters and modelling results are given in the Appendix.

Fig. 4 (a) Re concentrations versus Os concentrations and (b) $^{187}Os/^{188}Os$ ratios versus Os contents of the Hainan basalts compared with 3–17 Ma seamount basalts from the Philippine Sea plate (PSP) (Dale et al., 2008), the Hawaiian plume-induced lavas (Ireland et al., 2011; Ireland et al., 2009; Lassiter and Hauri, 1998; Lassiter et al., 2000) and early (ca. 60 Ma) Iceland plume-induced picrites from Baffin Island and west Greenland (BIWG) (Dale et al., 2009; Kent et al., 2004; Schaefer et al., 2000). PUM in (b) indicates putative present-day primitive upper mantle with $^{187}Os/^{188}Os$ = 0.1296 ± 0.0008 (Meisel et al., 2001). The $^{187}Os/^{188}Os$ ratios in (b) for the Hawaiian and the Iceland plume lavas have been corrected to their initial values**.** Data for abyssal peridotite (A.P.) in (b) are from Liu et al. (2008) and Dale et al. (2009). (c) $^{187}Os/^{188}Os$ versus $^{187}Re/^{188}Os$ and (d) $^{187}Os/^{188}Os$ versus Fe/Mn (Wang et al., 2012) for the Hainan basalts. The Hainan basalts have low Re contents compared to MORB (Gannoun et al., 2007; Schiano et al., 1997) and plot in the fields of OIB and high-magnesian samples (modified after Shirey and Walker, 1998). The error bars in (c) indicate 2 standard error (2 SE). The correlation of $^{187}Os/^{188}Os$ versus $^{187}Re/^{188}Os$ is likely due to melt mixing or crustal contamination. With the exceptions of two low-Os samples (08HN-5F and 08HN-14A), the remainder are scatter and broadly plot along the isochron of 22 Ma, suggesting an insignificant effect of crustal contamination on most samples.

Fig. 5 Plots of Sm/Nd and La/Sm against (a) and (b) Os concentration and (c) and (d) $^{187}Os/^{188}Os$ ratio. The open red circles in (a) and (b) indicate the data points that were excluded in calculating the least square linear regression lines (dashed lines). The composition of recycled oceanic crust and the bulk continental crust is from Stracke et al. (2003) and Rudnick and Gao (2003), respectively. The black solid lines with arrows represent crustal contamination trends.

Fig. 6 Plots of (a) La/Sm and (b) SiO_2 against Sm/Nd ratios for the LIS basalts. The chondritic bulk silicate Earth (BSE; McDonough and Sun, 1995), nonmodal batch partial melting (solid lines with squares or circles) and binary mixing (dark blue dashed lines) are shown. The modelling parameters for nonmodal partial melting are from Stracke et al. (2003). Recycled oceanic crust (ROC) is composed of 25%N-MORB (Hofmann, 1988) + 25%altered MORB (Staudigel et al., 1995) + 50%gabbro (Hart et al., 1999) with 1.93 ppm La, 7.37 ppm Nd, 2.45 ppm Sm. The recycled oceanic crust has 51 wt.% SiO_2, similar to primitive MORB (Kelemen et al., 2007). The peridotite-derived melt represents the enriched end-member (La = 3.7 ppm, Nd = 3.85 ppm, Sm = 1.27 ppm, SiO_2 = 44 wt.%). Partial melts of gabbros were experimentally determined (C-1913; Yaxley and Sobolev, 2007). Each filled circle or square on the partial melting lines in (a) represents a 5% increment of the melting fraction. Each cross on the binary mixing lines in (b) indicates 0.1 increments of recycled components. It should be pointed out that binary mixing between high melting of recycled oceanic crust (65%) and low (about 5–8%) to intermediate (15%) melting of peridotite is not a unique way to produce the correlation between SiO_2 and Sm/Nd in (b) because either the source heterogeneity (e.g., Hauri, 1996; Sobolev et al., 20005; Wang et al., 2012) or the melting conditions (e.g., Albarède, 1992; Haase, 1996; Walter, 1998) can contribute to variations in major element compositions. For example, SiO_2 content in melts of peridotitic sources correlates positively with melt fraction at intermediate melt fractions (0–40%; Walter, 1998) and negatively with melting pressure (Albarède, 1992; Haase, 1996). In addition, Sm/Nd ratio in melts also increases with increasing melt fraction because the bulk partition coefficient for Sm/Nd between melt and solid during partial melting of peridotitic sources is higher than 1 (e.g., Workman and Hart, 2005). Thus, changing melt fraction can also produce such a positive correlation. Furthermore, the inferred residual mineral assemblages indicate that the source of the high-silica melts (tholeiites) should be dominantly peridotite (Wang et al., 2012). The mineral/melt partition coefficients and melting proportions used in the non-modal batch partial melting calculations are presented in the Appendix. Data sources are the same as Fig. 3.

Fig. 7 (a) Evolution of MORB, gabbro and complete oceanic crust in $^{187}Os/^{188}Os$–$^{206}Pb/^{204}Pb$ space, (b) mixing peridotite mantle ($^{187}Os/^{188}Os$ = 0.123, $^{206}Pb/^{204}Pb$ = 18.7, Os = 3.1 ppb, Pb = 0.03 ppm) and recycled oceanic crust (50% MORB + 50% gabbro, Pb = 0.09 ppm, Os = 0.045 ppb), and gabbro (Pb = 0.114 ppm, Os = 0.055 ppb), and (c) mixing between peridotite-derived melts (Os = 0.5 ppb, Pb = 1.0 ppm) and partial melts of recycled oceanic crust (Pb = 0.54 ppb, Os = 0.045 ppb) and recycled gabbro (Pb = 0.172 ppm, Os = 0.055 ppb), (d) plot of $^{187}Os/^{188}Os$ against Sr/Sr*. Sr*/Sr = $Sr_N/(Ce_N \times Nd_N)^{0.5}$ (subscript N indicates primitive mantle normalized values). The bulk recycled oceanic crust (50% MORB + 50% gabbro) has $^{206}Pb/^{204}Pb$ and $^{187}Os/^{188}Os$ isotopic ratios at 0.1 Ga, 0.3 Ga and 0.5 Ga as follows: 18.39, 18.71, 19.04 and 0.493, 1.197, 1.903. Similarly, $^{206}Pb/^{204}Pb$ = 18.16, 18.03, 17.89 and $^{187}Os/^{188}Os$ = 0.315, 0.662, 1.01 for recycled gabbro according to recycling age in 0.1 Ga, 0.3 Ga, and 0.5 Ga. The Os concentrations for bulk oceanic crust and oceanic crust gabbro are from Peucker-Ehrenbrink et al. (2012). The fields of enriched plume mantle (EP) and EM2-type OIBs are modified after Shirey and Walker (1998). Data source for Sr, Ce and Nd data of Gabbro: average Gabal Gerf gabbro (Zimmer et al., 1995); average gabbro, 735B (Hart et al., 1999).

Fig. 8 A carton model illustrating the formation mechanism of the Hainan plume based on both seismic imaging results (Huang and Zhao, 2006; Lebedev and Nolet, 2003; Lei et al., 2009; Montelli et al., 2006; Wang and Huang, 2012; Zhao, 2007) and this study. Broad low velocity anomalies beneath the lithosphere and the transition zone are prominent in this region (Huang and Zhao, 2006; Lebedev and Nolet, 2003; Li et al., 2008a; Zhao, 2007), but the interpreted secondary plumes beneath the Indochina peninsula volcanic province and seamounts in the South China Sea (SCS) have not been reported in seismic tomographic data yet. The volcanism in the Indochina peninsula and the South China Sea may have been caused by past thermal plumes, or small-scale thermal upwellings from the edge of the broad anomaly. The possible lower mantle chemical domains is drawn according to the upside-down differentiation model (Lee et al., 2010), early silicate reservoirs recognized in plume-induced basaltic rocks (Jackson and Carlson, 2011; Jackson et al., 2010), and chemical-thermal properties of plumes (Campbell and O'Neill, 2012; Griffiths and Campbell, 1990).

References

Albarède, F., 1992, How deep do common basaltic magmas form and differentiate?: J. Geophys. Res. 97, 10997-11009.

Allegre, C.J., Lewin, E., 1995. Isotopic systems and stirring times of the earth's mantle. Earth Planet. Sci. Lett. 136, 629-646.

Anderson, D.L., 1982. Isotopic evolution of the mantle: the role of magma mixing. Earth Planet. Sci. Lett. 57, 1-12.

Andreasen, R., Sharma, M., Subbarao, K.V., Viladkar, S.G., 2008. Where on Earth is the enriched Hadean reservoir? Earth Planet. Sci. Lett. 266, 14-28.

Becker, H., 2000. Re–Os fractionation in eclogites and blueschists and the implications for recycling of oceanic crust into the mantle. Earth Planet. Sci. Lett. 177, 287-300.

Bourdon, B., Touboul, M., Caro, G., Kleine, T., 2008. Early differentiation of the Earth and the Moon. Phil. Trans. R. Soc. A366, 4105-4128.

Braitenberg, C., Wienecke, S., Wang, Y., 2006. Basement structures from satellite-derived gravity field: South China Sea ridge. J. Geophys. Res. 111, B05407.

Burke, K., Torsvik, T.H., 2004. Derivation of Large Igneous Provinces of the past 200 million years from long-term heterogeneities in the deep mantle. Earth Planet. Sci. Lett. 227, 531-538.

Campbell, I.H., Griffiths, R.W., 1990. Implications of mantle plume structure for the evolution of flood basalts. . Earth Planet. Sci. Lett. 99, 79-93.

Campbell, I.H., Griffiths, R.W., 1992. The changing nature of mantle hotspots through time: implications for the chemical evolution of the mantle. J.Geology 92, 497-523.

Campbell, I.H., O'Neill, S.C.H., 2012. Evidence against a chondritic Earth. Nature 483, 553-558.

Cao, Q., van der Hilst, R.D., de Hoop, M.V., Shim, S.-H., 2011. Seismic Imaging of Transition Zone Discontinuities Suggests Hot Mantle West of Hawaii. Science 332, 1068-1071.

Carlson, R.W., Boyet, M., 2008. Composition of the Earth's interior: the importance of early events. Phil. Trans. R. Soc. A 366, 4077-4103.

Caro, G., Bourdon, B., 2010. Non-chondritic Sm/Nd ratio in the terrestrial planets: Consequences for the geochemical evolution of the mantle-crust system. Geochim. Cosmochim. Acta 74, 3333-3349.

Coltice, N., Moreira, M., Hernlund, J., Labrosse, S., 2011. Crystallization of a basal magma ocean recorded by Helium and Neon. Earth Planet. Sci. Lett. 308, 193-199.

Courtillot, V., Davaille, A., Besse, J., Stock, J., 2003. Three distinct types of hotspots in the Earth's mantle. Earth and Planet. Sci. Lett. 205, 295-308.

Creaser, R.A., Papanastassiou, D.A., Wasserburg, G.J., 1991. Negative thermal ion mass spectrometry of osmium, rhenium and iridium. Geochim. Cosmochim. Acta 55, 397-401.

Dale, C.W., Gannoun, A., Burton, K.W., Argles, T.W., Parkinson, I.J., 2007. Rhenium-osmium isotope and elemental behaviour during subduction of oceanic crust and the implications for mantle recycling. Earth Planet. Sci. Lett. 253, 211-225.

Dale, C.W., Luguet, A., Macpherson, C.G., Pearson, D.G., Hickey-Vargas, R., 2008. Extreme platinum-group element fractionation and variable Os isotope compositions in Philippine Sea Plate basalts: Tracing mantle source heterogeneity. Chem. Geol. 248, 213-238.

Dale, C.W., Pearson, D.G., Starkey, N.A., Stuart, F.M., Ellam, R.M., Larsen, L.M., Fitton, J.G., Macpherson, C.G., 2009. Osmium isotopes in Baffin Island and West Greenland picrites: Implications for the 187Os/188Os composition of the convecting mantle and the nature of high 3He/4He mantle. Earth Planet. Sci. Lett. 278, 267-277.

Davies, J.H., Bunge, H.-P., 2006. Are splash plumes the origin of minor hotspots? Geology 34, 349-352.

Davis, F.A., Hirschmann, M.M., Humayun, M., 2011. The composition of the incipient partial melt of garnet peridotite at 3 GPa and the origin of OIB. Earth Planet. Sci. Lett. 308, 380-390.

Demény, A., Vennemann, T.W., Hegner, E., Ahijado, A., Casillas, R., Nagy, G., Homonnay, Z., Gutierrez, M., Szabó, C., 2004. H, O, Sr, Nd, and Pb isotopic evidence for recycled oceanic crust in the Transitional Volcanic Group of Fuerteventura, Canary Islands, Spain. Chem.Geol. 205, 37-54.

Flower, M.F.J., Zhang, M., Chen, C.-Y., Tu, K., Xie, G., 1992. Magmatism in the South China Basin : 2. Post-spreading Quaternary basalts from Hainan Island, south China. Chem.Geol. 97, 65-87.

Fukao, Y., Obayashi, M., Nakakuki, T., 2009. Stagnant Slab: A Review. Annu. Rev. Earth Planet. Sci. 37, 19-46.

Fukao, Y., Widiyantoro, S., Obayashi, M., 2001. Stagnant slabs in the upper and lower mantle transition region. Rev. Geophys. 39, 291-323.

Gannoun, A., Burton, K.W., Parkinson, I.J., Alard, O., Schiano, P., Thomas, L.E., 2007. The scale and origin of the osmium isotope variations in mid-ocean ridge basalts. Earth Planet. Sci. Lett. 259, 541-556.

Griffiths, R.W., Campbell, I.H., 1990. Stirring and structure in mantle starting plumes. Earth Planet. Sci. Lett. 99, 66-78.

Haase, K. M., 1996, The relationship between the age of the lithosphere and the composition of oceanic magmas: Constraints on partial melting, mantle sources and the thermal structure of the plates: Earth Planet. Sci. Lett.144, 75-92.

Han, J.W., Xiong, X.L., Zhu, Z.Y., 2009. Geochemistry of Late-Cenozoic basalts from Leiqiong area: The origin of EM2 and the contribution from sub-continental lithosphere mantle. Acta Petrologica Sinica 25, 3208-3220 (in Chinese with English abstract).

Hart, S.R., Blusztajn, J., Dick, H.J.B., Meyer, P.S., Muehlenbachs, K., 1999. The fingerprint of seawater circulation in a 500-meter section of ocean crust gabbros. Geochim. Cosmochim. Acta 63, 4059-4080.

Hart, S.R., Hauri, E.H., Oschmann, L.A., Whitehead, J.A., 1992. Mantle Plumes and Entrainment: Isotopic Evidence. Science 256, 517-520.

Hauri, E.H., 1996. Major-element variability in the Hawaiian mantle plume. Nature 382, 415-419.

Hauri, E.H., Whitehead, J.A., Hart, S.R., 1994. Fluid dynamic and geochemical aspects of entrainment in mantle plumes. J. Geophys. Res. 99, 24275-24300.

He, Y., Wen, L., 2011. Seismic velocity structures and detailed features of the D″ discontinuity near the core-mantle boundary beneath eastern Eurasia. Phys. Earth Planet. Inter. 189, 176-184.

Herzberg, C., Asimow, P.D., Arndt, N., Niu, Y., Lesher, C.M., Fitton, J.G., Saunders, A.D., 2007. Temperature in ambient mantle and plumes: Constraints from basalts,

picrites, and komatiites. Geochem. Geophys. Geosyst. 8, doi:10.1029/2006GC001390.
Ho, K.-s., Chen, J.-c., Juang, W.-s., 2000. Geochronology and geochemistry of late Cenozoic basalts from the Leiqiong area, southern China. J. Asian Earth Sci. 18, 307-324.
Hoang, N., Flower, M., 1998. Petrogenesis of Cenozoic Basalts from Vietnam: Implication for Origins of a 'Diffuse Igneous Province'. J. Petrol. 39, 369-395.
Hoang, N., Flower, M.F.J., Carlson, R.W., 1996. Major, trace element, and isotopic compositions of Vietnamese basalts: Interaction of hydrous EM1-rich asthenosphere with thinned Eurasian lithosphere. Geochim. Cosmochim. Acta 60, 4329-4351.
Hofmann, A.W., 1988. Chemical differentiation of the Earth: the relationship between mantle, continental crust, and oceanic crust. Earth Planet. Sci. Lett. 90, 297-314.
Hofmann, A.W., 1997. Mantle geochemistry: the message from oceanic volcanism. Nature 385, 219-229.
Hofmann, A. W., Jochum, K. P., Seufert, M., and White, W. M., 1986. Nb and Pb in oceanic basalts: new constraints on mantle evolution: Earth Planet. Sci. Lett.79, 33-45.
Hofmann, A.W., White, W.M., 1982. Mantle plumes from ancient oceanic crust. Earth Planet. Sci. Lett. 57, 421-436.
Huang, J., Zhao, D., 2006. High-resolution mantle tomography of China and surrounding regions. J. Geophys. Res. 111, B09305.
Huang, S., Frey, F., 2005. Recycled oceanic crust in the Hawaiian Plume: evidence from temporal geochemical variations within the Koolau Shield. Contrib. Mineral. Petrol. 149, 556-575.
Huang, Z., Wang, L., Zhao, D., Xu, M., Mi, N., Yu, D., Li, H., Li, C., 2010. Upper mantle structure and dynamics beneath Southeast China. Phys. Earth Planet. Inter. 182, 161-169.
Ireland, T.J., Walker, R.J., Brandon, A.D., 2011. 186Os-187Os systematics of Hawaiian picrites revisited: New insights into Os isotopic variations in ocean island basalts. Geochim. Cosmochim. Acta 75, 4456-4475.
Ireland, T.J., Walker, R.J., Garcia, M.O., 2009. Highly siderophile element and 187Os isotope systematics of Hawaiian picrites: Implications for parental melt composition and source heterogeneity. Chem. Geol. 260, 112-128.

Jackson, M.G., Carlson, R.W., 2011. An ancient recipe for flood-basalt genesis. Nature 476, 316-319.

Jackson, M.G., Carlson, R.W., 2012. Homogeneous superchondritic $^{142}Nd/^{144}Nd$ in the mid-ocean ridge basalt and ocean island basalt mantle. Geochem. Geophys. Geosyst. 13, Q06011.

Jackson, M.G., Carlson, R.W., Kurz, M.D., Kempton, P.D., Francis, D., Blusztajn, J., 2010. Evidence for the survival of the oldest terrestrial mantle reservoir. Nature 466, 853-856.

Jackson, M.G., Weis, D., Huang, S., 2012. Major element variations in Hawaiian shield lavas: Source features and perspectives from global ocean island basalt (OIB) systematics. Geochem. Geophys. Geosyst. 13, Q09009.

Kelemen, P.B., Hanghøj, K., Greene, A.R., 2007. 3.18 - One View of the Geochemistry of Subduction-Related Magmatic Arcs, with an Emphasis on Primitive Andesite and Lower Crust, in: Editors-in-Chief: Heinrich, D.H., Karl, K.T. (Eds.), Treatise on Geochemistry. Pergamon, Oxford, pp. 1-70.

Kent, A.J.R., Stolper, E.M., Francis, D., Woodhead, J., Frei, R., Eiler, J., 2004. Mantle heterogeneity during the formation of the North Atlantic Igneous Province: Constraints from trace element and Sr-Nd-Os-O isotope systematics of Baffin Island picrites. Geochem. Geophys. Geosyst. 5, Q11004.

Kogiso, T., Hirschmann, M.M., 2006. Partial melting experiments of bimineralic eclogite and the role of recycled mafic oceanic crust in the genesis of ocean island basalts. Earth Planet. Sci. Lett. 249, 188-199.

Kokfelt, T.F., Hoernle, K.A.J., Hauff, F., Fiebig, J., Werner, R., Garbe-Schonberg, D., 2006. Combined Trace Element and Pb-Nd–Sr-O Isotope Evidence for Recycled Oceanic Crust (Upper and Lower) in the Iceland Mantle Plume. J. Petrol. 47, 1705-1749.

Lassiter, J.C., Hauri, E.H., 1998. Osmium-isotope variations in Hawaiian lavas: evidence for recycled oceanic lithosphere in the Hawaiian plume. Earth Planet. Sci. Lett. 164, 483-496.

Lassiter, J.C., Hauri, E.H., Reiners, P.W., Garcia, M.O., 2000. Generation of Hawaiian post-erosional lavas by melting of a mixed lherzolite/pyroxenite source. Earth Planet. Sci. Lett. 178, 269-284.

Lebedev, S., Nolet, G., 2003. Upper mantle beneath Southeast Asia from S velocity tomography. J. Geophys. Res. 108, 2048.

Lee, C.-T.A., Luffi, P., Hoink, T., Li, J., Dasgupta, R., Hernlund, J., 2010. Upside-down differentiation and generation of a 'primordial' lower mantle. Nature 463, 930-933.

Lee, C.-T.A., Luffi, P., Plank, T., Dalton, H., Leeman, W.P., 2009. Constraints on the depths and temperatures of basaltic magma generation on Earth and other terrestrial planets using new thermobarometers for mafic magmas. Earth Planet. Sci. Lett. 279, 20-33.

Lei, J., Zhao, D., Steinberger, B., Wu, B., Shen, F., Li, Z., 2009. New seismic constraints on the upper mantle structure of the Hainan plume. Phys. Earth Planet. Inter. 173, 33-50.

Li, C., van der Hilst, R.D., Engdahl, E.R., Burdick, S., 2008a. A new global model for P wave speed variations in Earth's mantle. Geochem. Geophys. Geosyst. 9, Q05018.

Li, X.-H., Liu, D., Sun, M.I.N., Li, W.-X., Liang, X.-R., Liu, Y., 2004. Precise Sm-Nd and U-Pb isotopic dating of the supergiant Shizhuyuan polymetallic deposit and its host granite, SE China. Geol. Mag. 141, 225-231.

Li, Z.X., Bogdanova, S.V., Collins, A.S., Davidson, A., De Waele, B., Ernst, R.E., Fitzsimons, I.C.W., Fuck, R.A., Gladkochub, D.P., Jacobs, J., Karlstrom, K.E., Lu, S., Natapov, L.M., Pease, V., Pisarevsky, S.A., Thrane, K., Vernikovsky, V., 2008b. Assembly, configuration, and break-up history of Rodinia: A synthesis. Precambrian Research 160, 179-210.

Li, Z.-X., Zhong, S., 2009. Supercontinent-superplume coupling, true polar wander and plume mobility: Plate dominance in whole-mantle tectonics. Phys. Earth Planet. Inter. 176, 143-156.

Liu, C.-Z., Snow, J.E., Hellebrand, E., Brugmann, G., von der Handt, A., Buchl, A., Hofmann, A.W., 2008. Ancient, highly heterogeneous mantle beneath Gakkel ridge, Arctic Ocean. Nature 452, 311-316.

Mallik, A., Dasgupta, R., 2012. Reaction between MORB-eclogite derived melts and fertile peridotite and generation of ocean island basalts. Earth Planet. Sci. Lett. 329–330, 97-108.

Maruyama, S., 1994. Plume tectonics. J. Geol. Soc. Japan 100, 24– 49.

McDonough, W.F., Sun, S.s., 1995. The composition of the Earth. Chem. Geol. 120, 223-253.

Meisel, T., Walker, R.J., Irving, A.J., Lorand, J.-P., 2001. Osmium isotopic compositions of mantle xenoliths: a global perspective. Geochim. Cosmochim. Acta 65, 1311-1323.

Meyzen, C.M., Blichert-Toft, J., Ludden, J.N., Humler, E., Mevel, C., Albarede, F., 2007. Isotopic portrayal of the Earth's upper mantle flow field. Nature 447, 1069-1074.

Miller, G.H., Stolper, E.M., Ahrens, T.J., 1991. The equation of state of a molten komatiite. 2. Application to komatiite petrogenesis and the Hadean mantle. J. Geophys. Res. 96, 11849-11864.

Montelli, R., Nolet, G., Dahlen, F.A., Masters, G., 2006. A catalogue of deep mantle plumes: New results from finite-frequency tomography. Geochem. Geophys. Geosyst. 7, Q11007.

Niu, Y., O'Hara, M.J., 2003. Origin of ocean island basalts: A new perspective from petrology, geochemistry, and mineral physics considerations. J. Geophys. Res. 108, 2209.

Nomura, R., Ozawa, H., Tateno, S., Hirose, K., Hernlund, J., Muto, S., Ishii, H., Hiraoka, N., 2011. Spin crossover and iron-rich silicate melt in the Earth's deep mantle. Nature 473, 199-202.

O'Neill, H.S.C., Palme, H., 2008. Collisional Erosion and the Non-Chondritic Composition of the Terrestrial Planets. Phil. Trans. R. Soc. A 366, 4205-4238.

Ogawa, M., 2010. Variety of plumes and the fate of subducted basaltic crusts. Phys. Earth Planet. Inter. 183, 366-375.

Pearson, D.G., Woodland, S.J., 2000. Solvent extraction/anion exchange separation and determination of PGEs (Os, Ir, Pt, Pd, Ru) and Re–Os isotopes in geological samples by isotope dilution ICP-MS. Chem. Geol. 165, 87-107.

Peucker-Ehrenbrink, B., Hanghoj, K., Atwood, T., Kelemen, P.B., 2012. Rhenium-osmium isotope systematics and platinum group element concentrations in oceanic crust. Geology 40, 199-202.

Rapp, R.P., Irifune, T., Shimizu, N., Nishiyama, N., Norman, M.D., Inoue, T., 2008. Subduction recycling of continental sediments and the origin of geochemically enriched reservoirs in the deep mantle. Earth Planet. Sci. Lett. 271, 14-23.

Rudnick, R.L., Gao, S., 2003. Composition of the continental crust, in: Rudnick, R.L. (Ed.), The Crust. Elsevier-Pergamon,Oxford, pp. 1-64.

Schaefer, B.F., Parkinson, I.J., Hawkesworth, C.J., 2000. Deep mantle plume osmium isotope signature from West Greenland Tertiary picrites. Earth Planet. Sci. Lett. 175, 105-118.

Schiano, P., Birck, J.-L., Allegre, C.J., 1997. Osmium-strontium-neodymium-lead isotopic covariations in mid-ocean ridge basalt glasses and the heterogeneity of the upper mantle. Earth Planet. Sci. Lett. 150, 363-379.

Shi, X., Kohn, B., Spencer, S., Guo, X., Li, Y., Yang, X., Shi, H., Gleadow, A., 2011. Cenozoic denudation history of southern Hainan Island, South China Sea: Constraints from low temperature thermochronology. Tectonophysics 504, 100-115.

Shirey, S.B., Walker, R.J., 1995. Carius Tube Digestion for Low-Blank Rhenium-Osmium Analysis. Anal. Chem. 67, 2136-2141.

Shirey, S.B., Walker, R.J., 1998. The Re-Os Isotope system in cosmochemistry and high-temeprature geochemistry. Annu. Rev. Earth Planet. Sci. 26, 423-500.

Sobolev, A.V., Hofmann, A.W., Jochum, K.P., Kuzmin, D.V., Stoll, B., 2011a. A young source for the Hawaiian plume. Nature 476, 434-437.

Sobolev, A.V., Hofmann, A.W., Kuzmin, D.V., Yaxley, G.M., Arndt, N.T., Chung, S.-L., Danyushevsky, L.V., Elliott, T., Frey, F.A., Garcia, M.O., Gurenko, A.A., Kamenetsky, V.S., Kerr, A.C., Krivolutskaya, N.A., Matvienkov, V.V., Nikogosian, I.K., Rocholl, A., Sigurdsson, I.A., Sushchevskaya, N.M., Teklay, M., 2007. The Amount of Recycled Crust in Sources of Mantle-Derived Melts. Science 316, 412-417.

Sobolev, A.V., Hofmann, A.W., Nikogosian, I.K., 2000. Recycled oceanic crust observed in `ghost plagioclase' within the source of Mauna Loa lavas. Nature 404, 986-990.

Sobolev, A.V., Hofmann, A.W., Sobolev, S.V., Nikogosian, I.K., 2005. An olivine-free mantle source of Hawaiian shield basalts. Nature 434, 590-597.

Sobolev, S.V., Sobolev, A.V., Kuzmin, D.V., Krivolutskaya, N.A., Petrunin, A.G., Arndt, N.T., Radko, V.A., Vasiliev, Y.R., 2011b. Linking mantle plumes, large igneous provinces and environmental catastrophes. Nature 477, 312-316.

Staudigel, H., Davies, G.R., Hart, S.R., Marchant, K.M., Smith, B.M., 1995. Large scale isotopic Sr, Nd and O isotopic anatomy of altered oceanic crust: DSDP/ODP sites417/418. Earth Planet. Sci. Lett. 130, 169-185.

Steinberger, B., Torsvik, T.H., 2012. A geodynamic model of plumes from the margins of Large Low Shear Velocity Provinces. Geochem. Geophys. Geosyst. 13, Q01W09.

Stolper, E., Walker, D., Hager, B.H., Hays, J.F., 1981. Melt segregation from partially molten source regions: the importance of melt density and source region size. J. Geophys. Res. 86, 6261-6271.

Stracke, A., Bizimis, M., Salters, V.J.M., 2003. Recycling oceanic crust: Quantitative constraints. Geochem. Geophys. Geosyst. 4, 8003.

Stracke, A., Hofmann, A.W., Hart, S.R., 2005. FOZO, HIMU, and the rest of the mantle zoo. Geochem. Geophys. Geosyst. 6, Q05007.

Stroncik, N.A., Devey, C.W., 2011. Recycled gabbro signature in hotspot magmas unveiled by plume-ridge interactions. Nature Geosci 4, 393-397.

Sun, S.S., 1980. Lead Isotopic Study of Young Volcanic Rocks from Mid-Ocean Ridges, Ocean Islands and Island Arcs. Phil. Trans. R. Soc. Lond. A297, 409-445.

Suzuki, A., Ohtani, E., Kato, T., 1998. Density and thermal expansion of a peridotite melt at high pressure. Phys. Earth Planet. Inter. 107, 53-61.

Tackley, P.J., 2011. Living dead slabs in 3-D: The dynamics of compositionally-stratified slabs entering a “slab graveyard” above the core-mantle boundary. Phys. Earth Planet. Inter.188, 150-162.

Takahahshi, E., Nakajima, K., Wright, T.L., 1998. Origin of the Columbia River basalts: melting model of a heterogeneous plume head. Earth Planet. Sci. Lett. 162, 63-80.

Tanaka, T., Togashi, S., Kamioka, H., Amakawa, H., Kagami, H., Hamamoto, T., Yuhara, M., Orihashi, Y., Yoneda, S., Shimizu, H., 2000. JNdi-1: a neodymium isotopic reference in consistency with LaJolla neodymium. Chem. Geol. 168, 279-281.

Tu, K., Flower, M.F.J., Carlson, R.W., Xie, G., Chen, C.-Y., Zhang, M., 1992. Magmatism in the South China Basin: 1. Isotopic and trace-element evidence for an endogenous Dupal mantle component. Chem. Geol. 97, 47-63.

Tu, K., Flower, M.F.J., Carlson, R.W., Zhang, M., Xie, G., 1991. Sr, Nd, and Pb isotopic compositions of Hainan basalts (south China): Implications for a subcontinental lithosphere Dupal source. Geology 19, 567-569.

van der Hilst, R.D., Widiyantoro, S., Engdahl, E.R., 1997. Evidence for deep mantle circulation from global tomography. Nature 386, 578-584.

Walter, M. J., 1998, Melting of Garnet Peridotite and the Origin of Komatiite and Depleted Lithosphere: J. Petrol. 39, 29-60.

Wang, C.-Y., Huang, J.-L., 2012. Mantle transition zone structure around Hainan by receiver function analysis. Chin. J Geophys. Ch 55, 1161-1167.

Wang, X.-C., Li, Z.-X., Li, X.-H., Li, J., Liu, Y., Long, W.-G., Zhou, J.-B., Wang, F., 2012. Temperature, Pressure, and Composition of the Mantle Source Region of Late Cenozoic Basalts in Hainan Island, SE Asia: a Consequence of a Young Thermal Mantle Plume close to Subduction Zones? J. Petrol. 53, 177-233.

White, W.M., 2010. Oceanic Island Basalts and Mantle Plumes: The Geochemical Perspective. Annu. Rev. Earth Planet. Sci. 38, 133-160.

Workman, R.K., Hart, S.R., 2005. Major and trace element composition of the depleted MORB mantle (DMM). Earth Planet. Sci. Lett. 231, 53-72.

Yan, P., Deng, H., Liu, H., Zhang, Z., Jiang, Y., 2006. The temporal and spatial distribution of volcanism in the South China Sea region. J. Asian Earth Sci. 27, 647-659.

Yan, Q., Shi, X., Wang, K., Bu, W., Xiao, L., 2008. Major element, trace element, and Sr, Nd and Pb isotope studies of Cenozoic basalts from the South China Sea. Sci. China Ser. D 51, 550-566.

Yaxley, G., Sobolev, A., 2007. High-pressure partial melting of gabbro and its role in the Hawaiian magma source. Contrib. Mineral. Petrol. 154, 371-383.

Yeh, Y.-C., Sibuet, J.-C., Hsu, S.-K., Liu, C.-S., 2010. Tectonic evolution of the Northeastern South China Sea from seismic interpretation. J. Geophys. Res. 115, B06103.

Zhang, N., Zhong, S., Leng, W., Li, Z.X., 2010. A model for the evolution of the earth's mantle structure since the early paleozoic. J. Geophys. Res. Solid Earth, 115, B06401, doi:http://dx.doi.org/10.1029/2009JB006896.

Zhao, D., 2004. Global tomographic images of mantle plumes and subducting slabs: insight into deep Earth dynamics. Phys. Earth Planet. Inter. 146, 3-34.

Zhao, D., 2007. Seismic images under 60 hotspots: Search for mantle plumes. Gondwana. Res. 12, 335-355.

Zhao, D., Yu, S., Ohtani, E., 2011. East Asia: Seismotectonics, magmatism and mantle dynamics. J. Asian Earth Sci. 40, 689-709.

Zhong, S., Zhang, N., Li, Z.-X., Roberts, J.H., 2007. Supercontinent cycles, true polar wander, and very long-wavelength mantle convection. Earth Planet. Sci. Lett. 261, 551-564.

Zhou, P., Mukasa, S.B., 1997. Nd-Sr-Pb isotopic, and major- and trace-element geochemistry of Cenozoic lavas from the Khorat Plateau, Thailand: sources and petrogenesis. Chem. Geol. 137, 175-193.

Zimmer, M., Kröner, A., Jochum, K.P., Reischmann, T., Todt, W., 1995. The Gabal Gerf complex: A precambrian N-MORB ophiolite in the Nubian Shield, NE Africa. Chem. Geol. 123, 29-51.

Zindler, A., Hart, S., 1986. Chemical geodynamics. Annu. Rev. Earth Planet. Sci. 14, 493-571.

Zou, H., Fan, Q., 2010. U-Th isotopes in Hainan basalts: Implications for sub-asthenospheric origin of EM2 mantle endmember and the dynamics of melting beneath Hainan Island. Lithos 116, 145-152.

***Highlights (for review)**

Highlights

- Late Cenozoic basalts in Southeast Asia display primitive Sr, Nd and Pb isotopes.
- Coexistence of a 4.5– 4.4 Ga-old reservoir and a minor young recycled component.
- Support dynamic linkages between deep subduction and mantle plume generation.

Graphical abstract

Formation mechanism of the Hainan plume close to major sudbuction systems

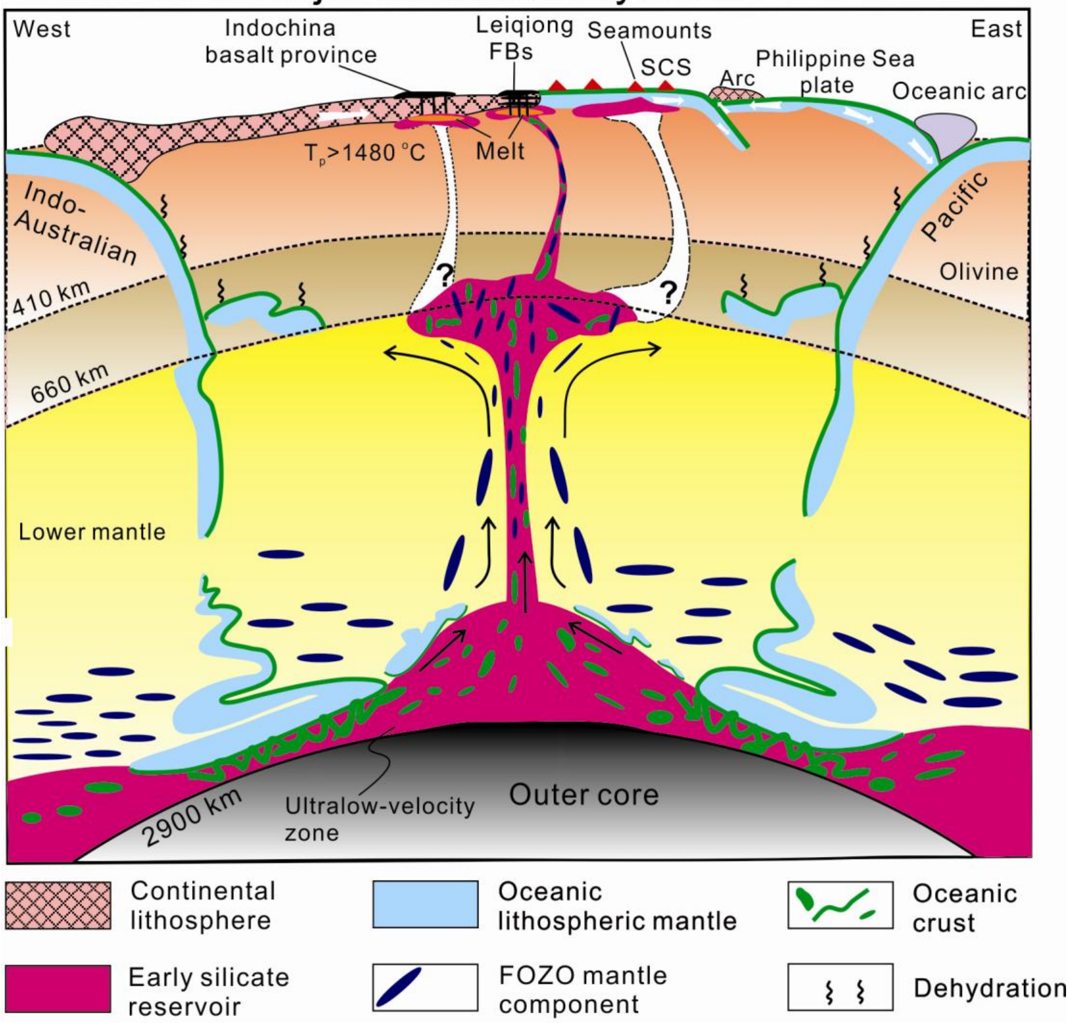

This study may provide the first observational support for dynamic linkage between deep subduction and mantle plume generation.

Figure-1
Click here to download Figure: Final Figure-July-2-1.pdf

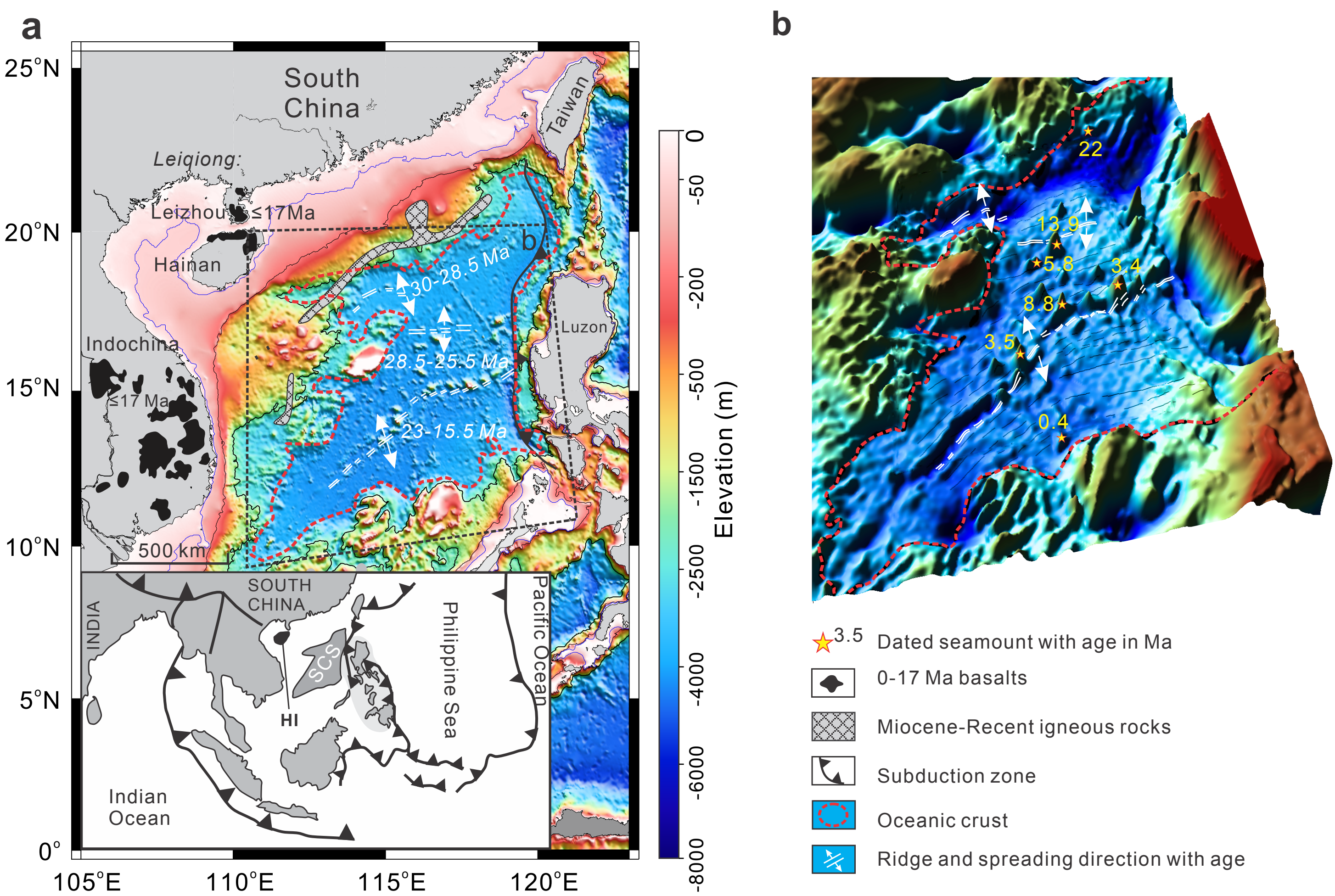

Figure-2

Click here to download Figure: Final Figure-July-2-2.eps

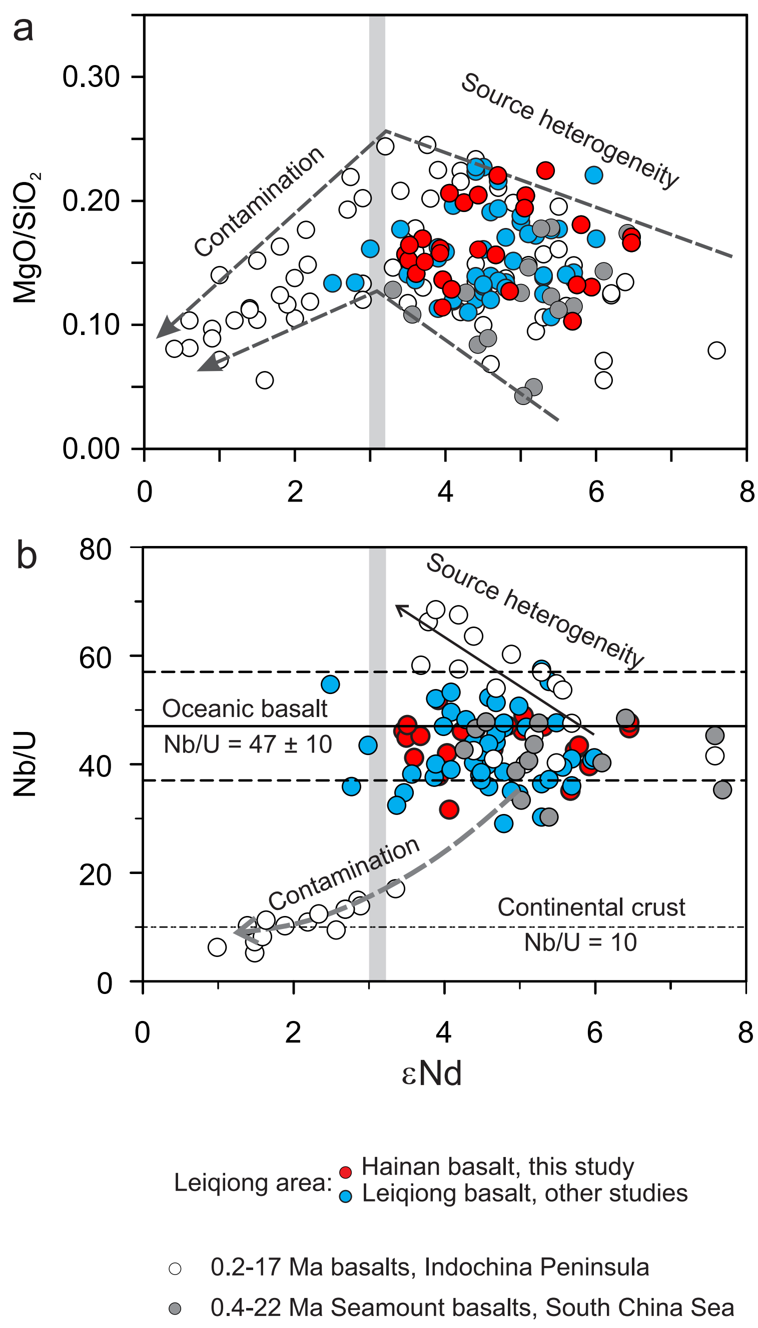

Figure-3

Click here to download Figure: Final Figure-July-2-3.eps

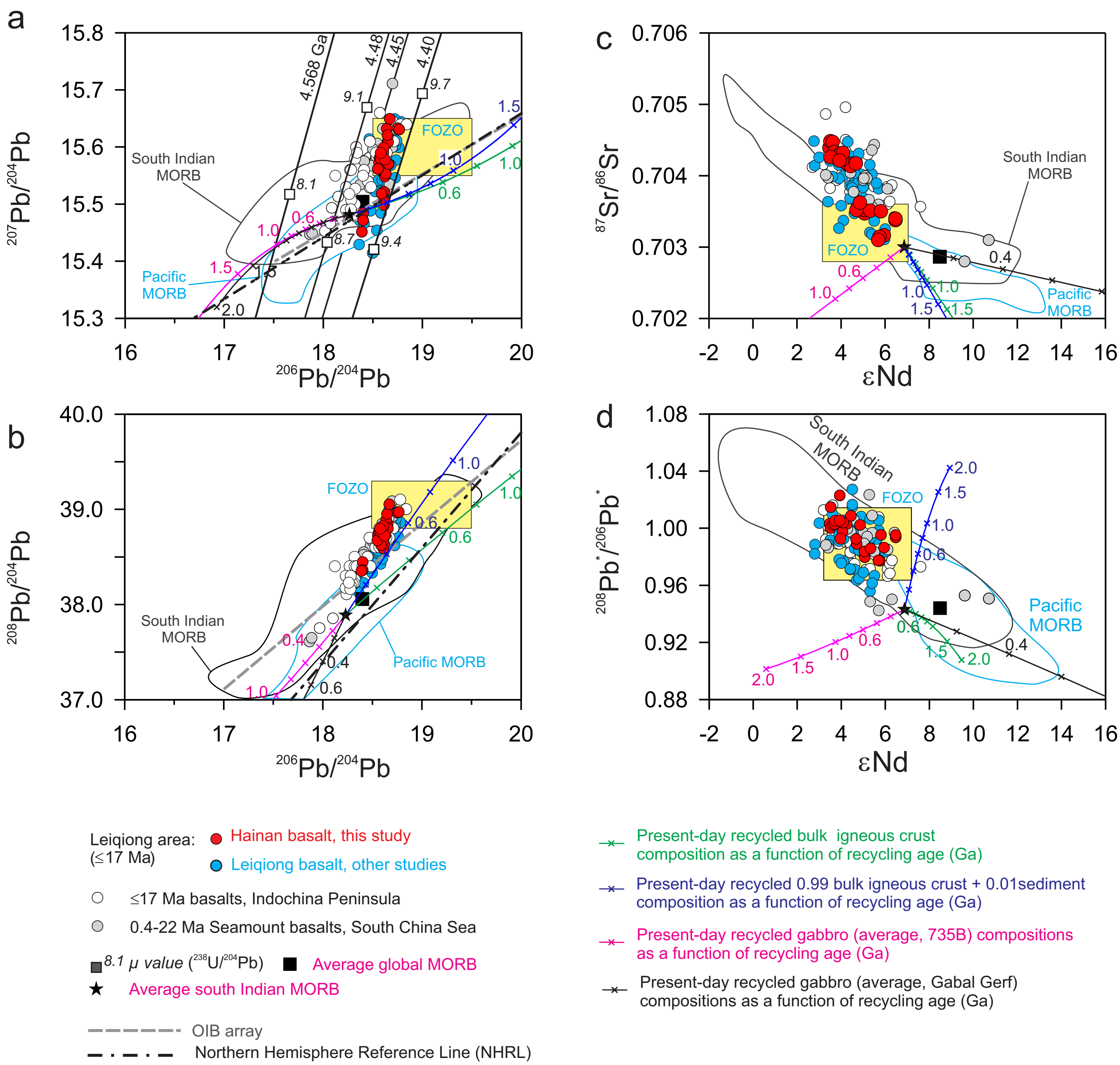

Figure-4

Click here to download Figure: Final Figure-July-2-4.eps

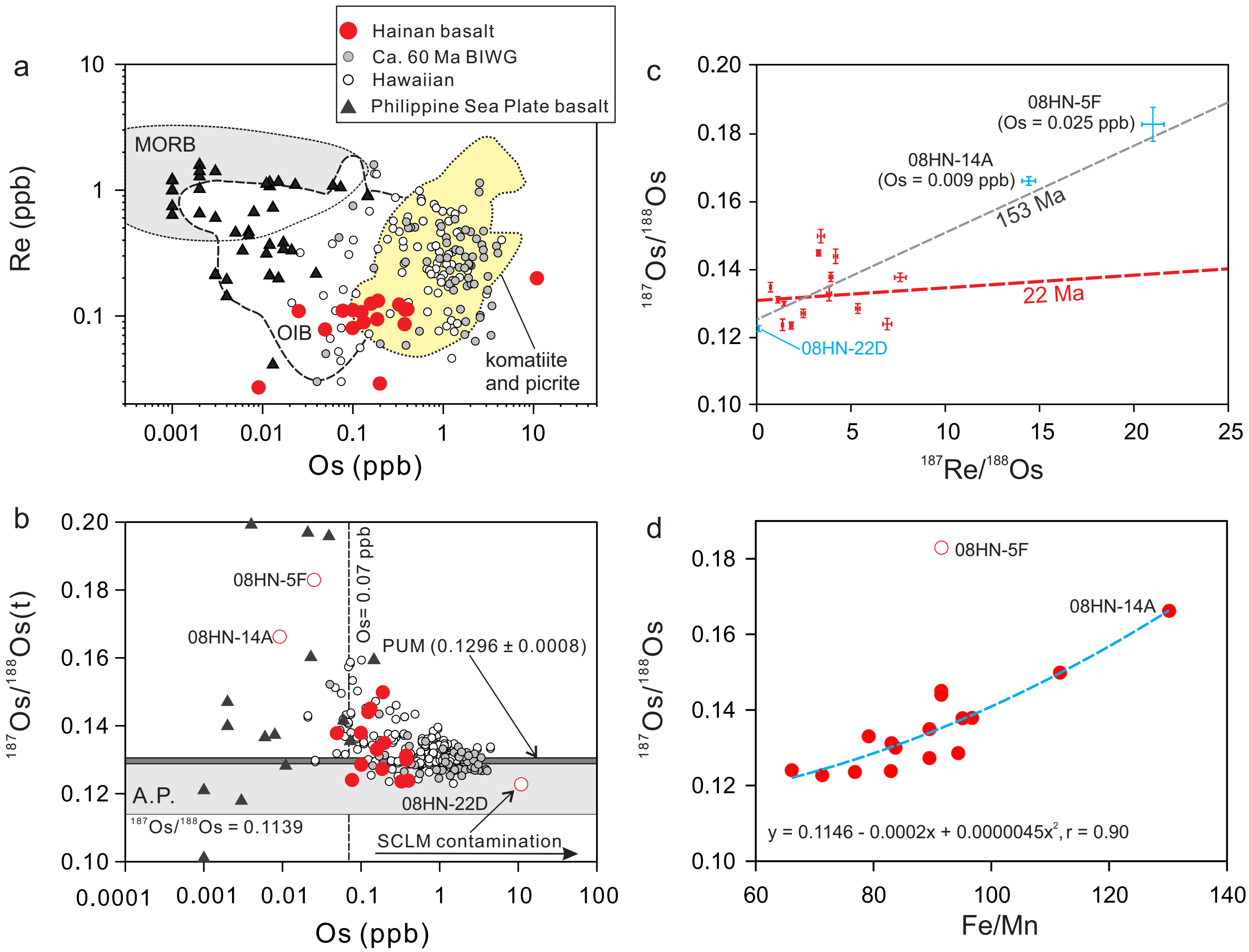

Figure-5

Click here to download Figure: Final Figure-July-2-5.eps

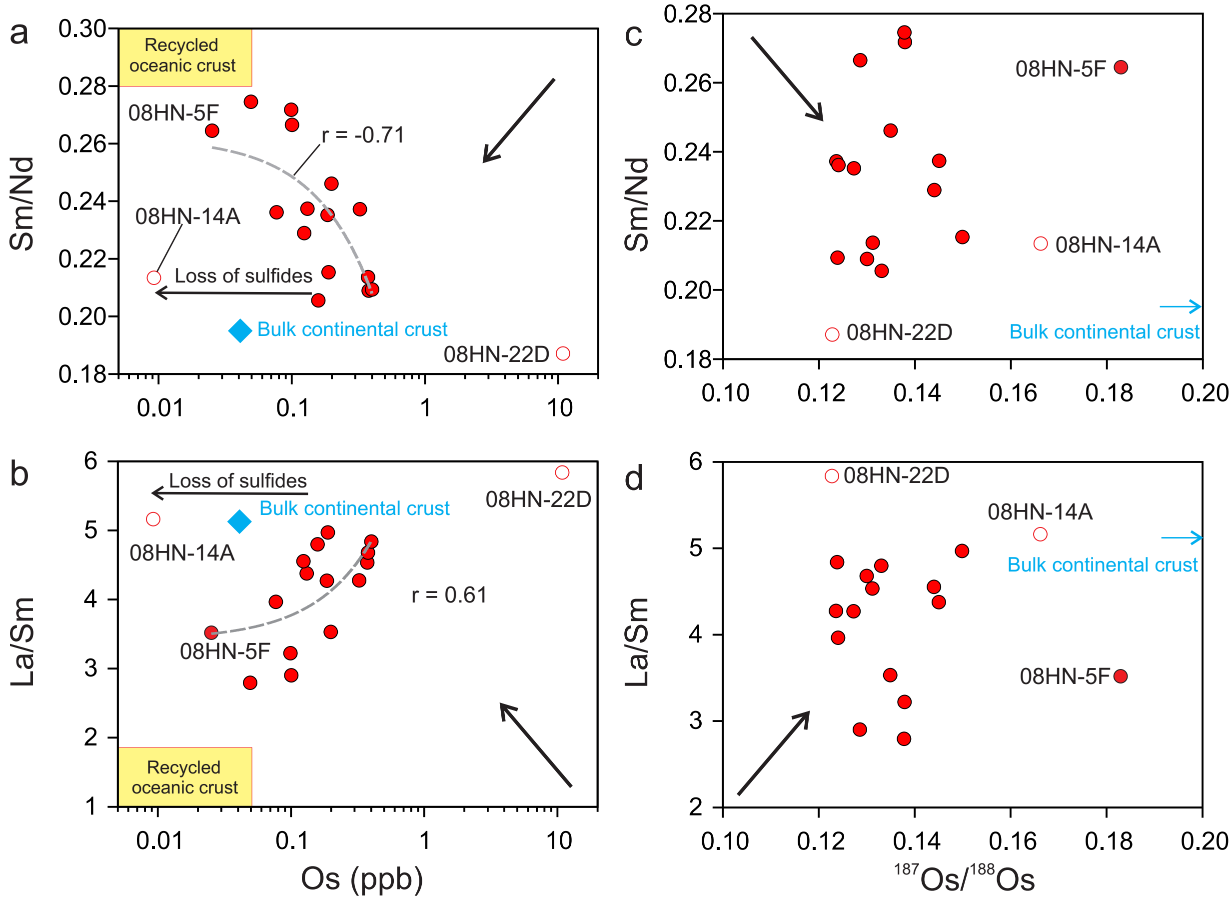

Figure-6
Click here to download Figure: Final Figure-July-2-6.eps

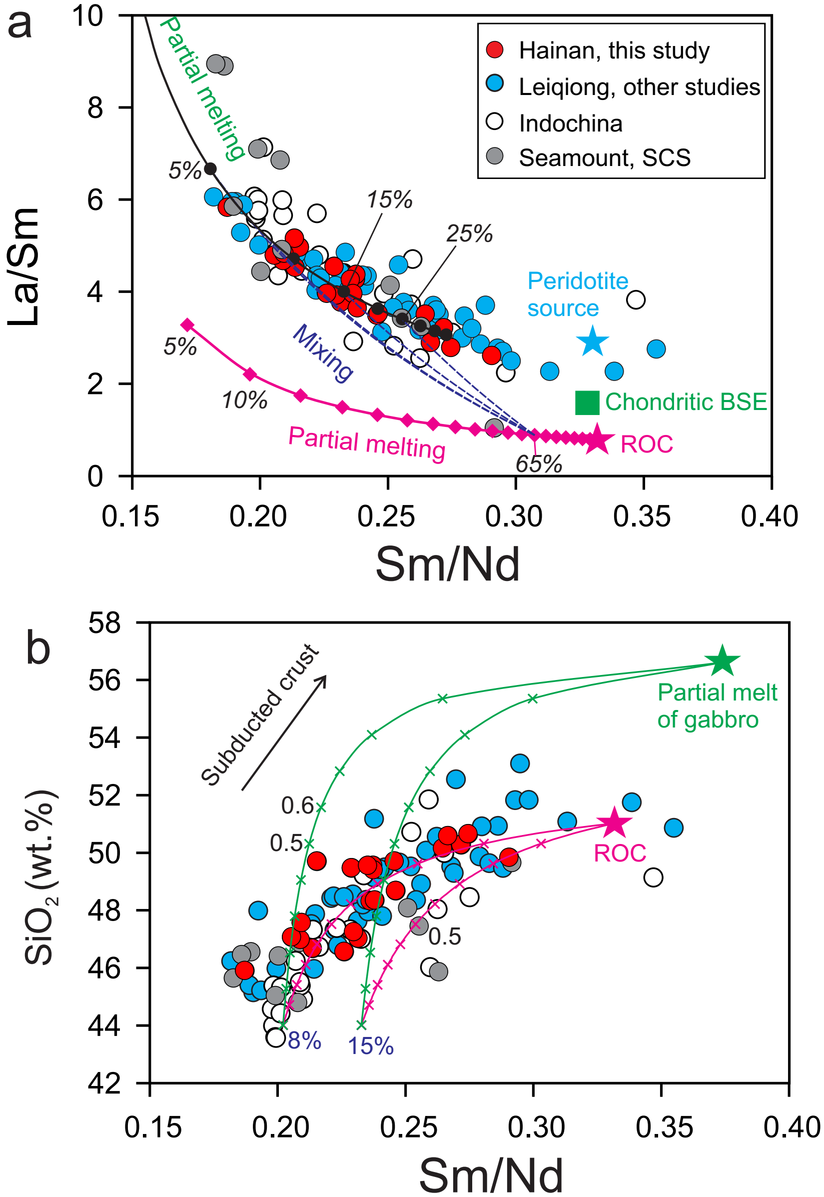

Figure-7

Click here to download Figure: Final Figure-July-2-7.eps

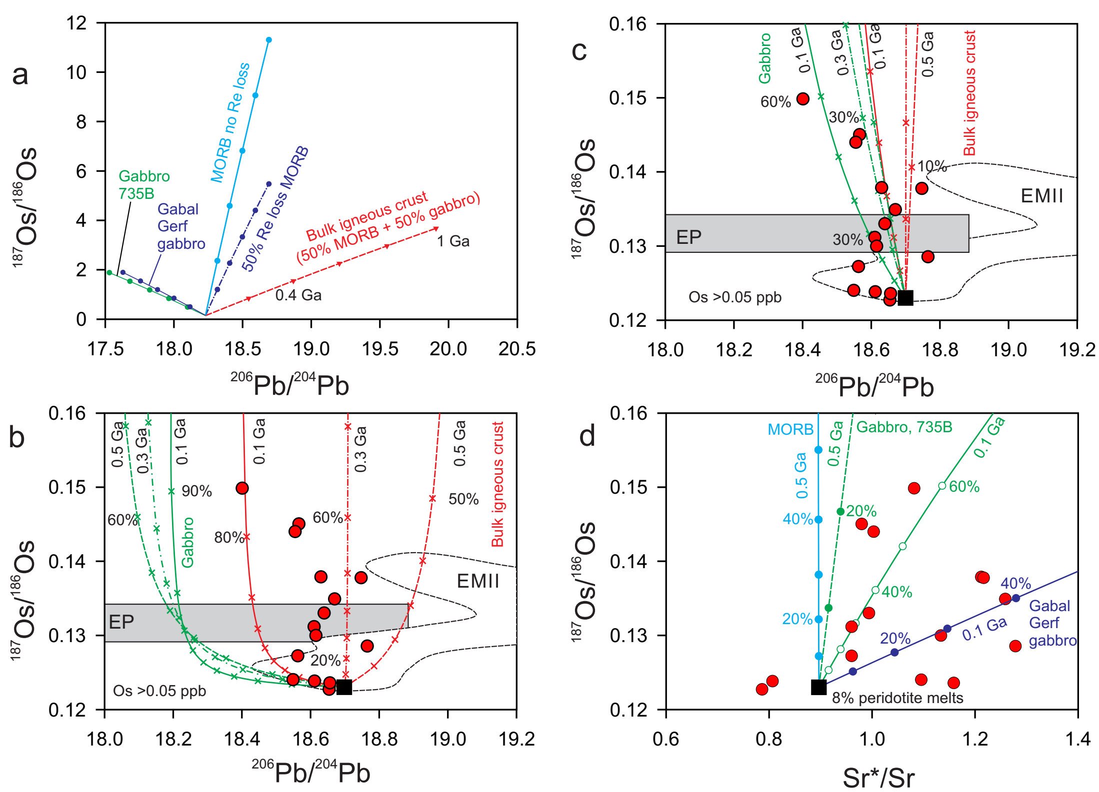

Figure-8

Click here to download Figure: Final Figure-July-2-8.pdf

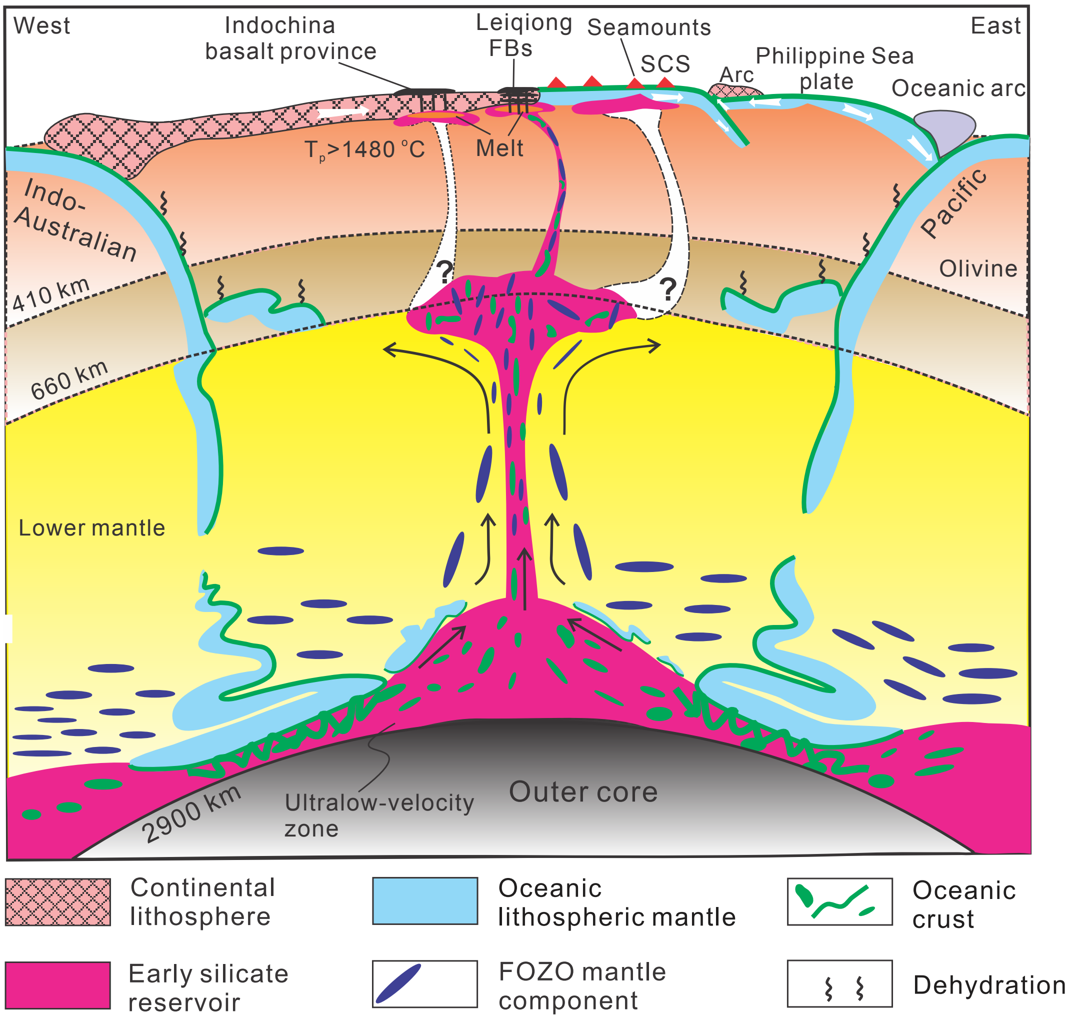

1. Supplementary Figures S1 to S3

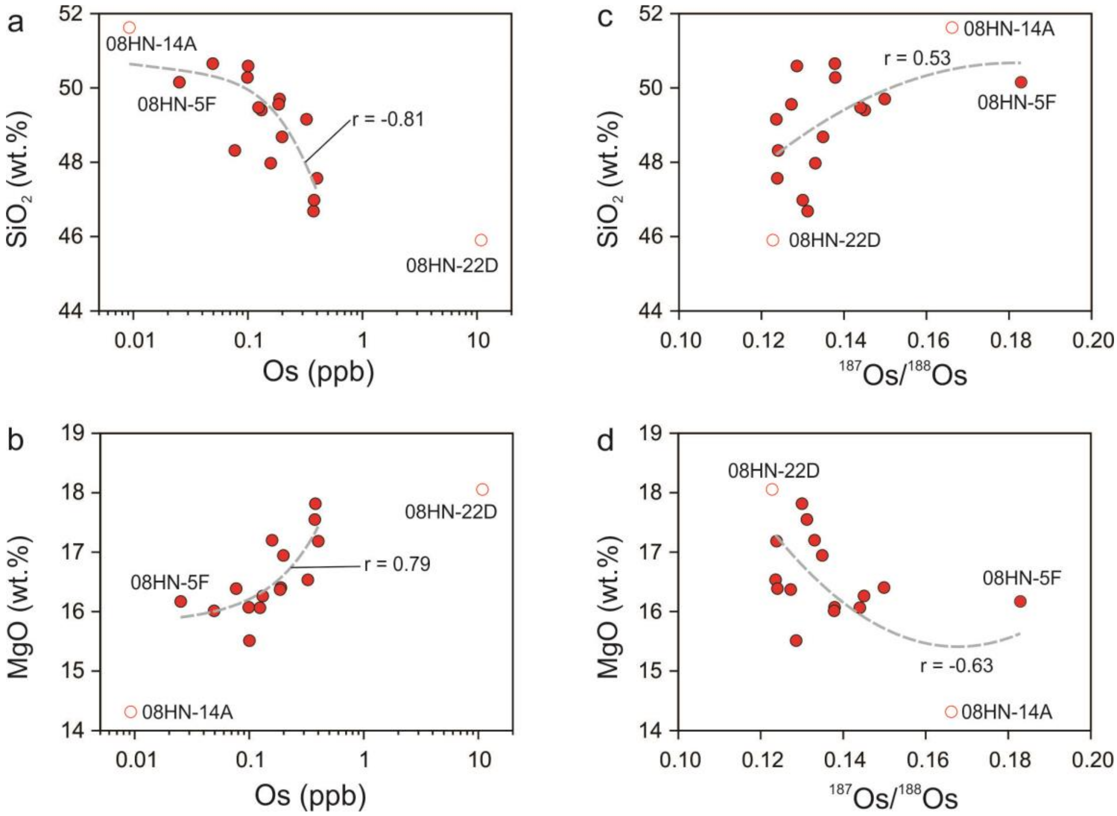

Fig. S1 Plots of SiO_2 and MgO against (a)–(b) Os concentration and (c)–(d) $^{187}Os/^{188}Os$. The open red circles indicate the data points are excluded in calculating the least square linear regression lines (dashed lines).

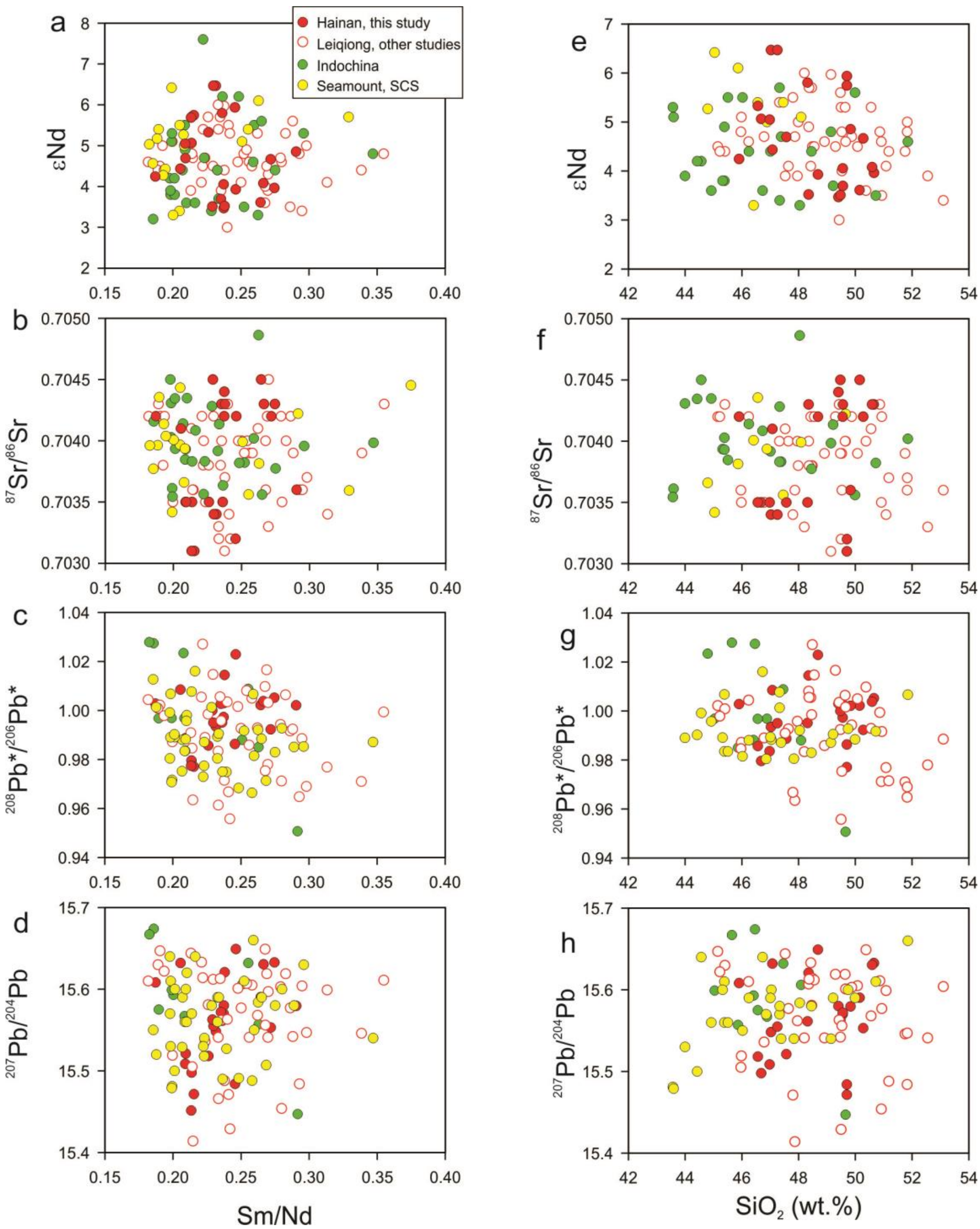

Fig. S2 Plots of εNd, $^{87}Sr/^{86}Sr$, $^{208}Pb^{*}/^{206}Pb^{*}$, and $^{207}Pb/^{204}Pb$ against (a)–(d) Sm/Nd and (e)–(h) SiO_2. The data source is same in main Fig. 2.

2. Supplementary Tables S1 to S3

Table S1 Re-Os isotope composition of the Hainan flood basalts (this study)

	Re (ppt)	2 SE	Os (ppt)	2 SE	$^{187}Os/^{188}Os$	2 SE	$^{187}Re/^{188}Os$	2 SE
Alkali basalt								
08HN-1A	113	3	400	9	0.12383	0.00169	1.36	0.05
08HN-2A	86	4	373	4	0.13116	0.00094	1.11	0.06
08HN-2B	112	3	377	4	0.12998	0.00066	1.43	0.04
08HN-16C	132	7	189	4	0.14986	0.00201	3.39	0.18
08HN-22D	199	8	10870	3064	0.12272	0.00092	0.09	0.03
08HN-24B	125	3	158	3	0.13302	0.00209	3.82	0.12
ZK03-24-4	111	2	100	1	0.12855	0.00145	5.35	0.12
Tholeiite								
08HN-4B	80	2	99	0	0.13789	0.00133	3.92	0.09
08HN-4D	123	5	324	4	0.12358	0.00101	1.82	0.08
08HN-5C	89	2	131	1	0.14503	0.00087	3.27	0.09
08HN-5E	107	2	124	2	0.14399	0.00212	4.17	0.11
08HN-5F	109	3	25	0	0.18292	0.00500	21.00	0.59
08HN-5J	94	3	185	5	0.12724	0.00126	2.45	0.10
08HN-8A	110	3	77	2	0.12401	0.00170	6.92	0.23
08HN-10B	78	3	49	0	0.13778	0.00127	7.60	0.31
08HN-14A	27	1	9	0	0.1662		14.41	0.58
08HN-25C	29	2	198	4	0.13491	0.00139	0.72	0.04

Table S2 Sr, Nd, and Pb isotope composition of the Hainan flood basalts (this study)

	$^{206}Pb/^{204}Pb$	2SE (%)	$^{207}Pb/^{204}Pb$	2SE (%)	$^{208}Pb/^{204}Pb$	2SE (%)	$^{87}Sr/^{86}Sr$	2SE	$^{143}Nd/^{144}Nd$	2SE	εNd
08HN-1A	18.6114674	0.014	15.52	0.015	38.67	0.016	0.70352	0.000014	0.512877	0.000006	4.69
08HN-2A	18.61	0.01	15.50	0.01	38.59	0.01	0.70347	0.000013	0.512896	0.000010	5.06
08HN-2B	18.62	0.015	15.51	0.015	38.63	0.016	0.70352	0.000010	0.512895	0.000007	5.05
08HN-3	18.59	0.011	15.52	0.013	38.62	0.015	0.70351	0.000011	0.512909	0.000007	5.33
08HN-4B	18.63	0.013	15.55	0.013	38.73	0.012	0.70417	0.000014	0.512875	0.000009	4.67
08HN-4D	18.66	0.013	15.57	0.013	38.80	0.015	0.70422	0.000015	0.512844	0.000008	4.05
08HN-5C	18.57	0.008	15.58	0.007	38.76	0.008	0.70439	0.000011	0.512814	0.000006	3.47
08HN-5E	18.55	0.017	15.56	0.017	38.72	0.017	0.70448	0.000014	0.512816	0.000008	3.51
08HN-5F	18.60	0.013	15.59	0.013	38.79	0.013	0.70447	0.000013	0.512821	0.000008	3.61
08HN-5J	18.56	0.015	15.57	0.014	38.76	0.014	0.70433	0.000011	0.512825	0.000008	3.69
08HN-8A	18.55	0.019	15.56	0.021	38.67	0.023	0.70350	0.000010	0.512933	0.000006	5.80
08HN-10B	18.75	0.019	15.63	0.019	38.96	0.023	0.70431	0.000015	0.512839	0.000007	3.96
08HN-11A	18.77	0.012	15.63	0.012	38.97	0.014	0.70432	0.000015	0.512845	0.000008	4.08
08HN-14A	18.39	0.011	15.45	0.011	38.35	0.011	0.70310	0.000014	0.512928	0.000008	5.69
08HN-16A	18.40	0.015	15.48	0.016	38.45	0.019	0.70316	0.000013	0.512940	0.000007	5.94
08HN-	18.40	0.014	15.47	0.014	38.36	0.014	0.70314	0.000013	0.512931	0.000006	5.74

16C											
08HN-18B	18.58	0.013	15.58	0.013	38.76	0.016	0.70362	0.000013	0.512885	0.000008	4.85
08HN-19A	18.62	0.016	15.55	0.015	38.73	0.015	0.70338	0.000014	0.512968	0.000006	6.47
08HN-19C	18.62	0.01	15.55	0.012	38.74	0.014	0.70340	0.000011	0.512968	0.000006	6.47
08HN-22D	18.65	0.01	15.61	0.01	38.85	0.009	0.70417	0.000011	0.512854	0.000008	4.24
08HN-24B	18.64	0.017	15.63	0.018	38.89	0.02	0.70413	0.000013	0.512863	0.000008	4.43
08HN-25A	18.65	0.017	15.62	0.02	38.95	0.023	0.70426	0.000014	0.512816	0.000008	3.52
08HN-25C	18.67	0.016	15.65	0.017	39.05	0.017	0.70421	0.000013	0.512837	0.000007	3.93
ZK03-29-1	18.59	0.015	15.51	0.015	38.70	0.014	0.70367	0.000010	0.512863	0.000006	4.43
ZK04-10-5	18.62	0.02	15.58	0.023	38.72	0.025			0.512839	0.000009	3.96
ZK05-21.1	18.61	0.019	15.60	0.02	38.82	0.022			0.512827	0.000009	3.72
ZK05-25-4	18.58	0.018	15.59	0.018	38.80	0.021			0.512837	0.000007	3.93

Table S3 Compilation Sr, Nd, and Pb isotopic data on late Cenozoic basalts in the Leiqiong and the Indochina peninsula, and on seamounts basalts in the South China Sea

	Ref.	SiO_2	MgO	$^{206}Pb/^{204}Pb$	$^{207}Pb/^{204}Pb$	$^{208}Pb/^{204}Pb$	$^{208}Pb^*/^{206}Pb^*$	$^{87}Sr/^{86}Sr$	$^{143}Nd/^{144}Nd$	εNd
Leiqiong flood basalts										
HXSF	1	50.4	6.9	18.58	15.54	38.61	0.986	0.70391	0.512875	4.6
HHLA-26	1	53.0	7.5	18.73	15.58	38.82	0.992	0.70420	0.512819	3.5
HQBA-10	1	50.7	6.8	18.53	15.53	38.59	0.989	0.70414	0.512783	2.8
HWNA	1	48.6	6.5	18.52	15.52	38.52	0.982	0.70448	0.512768	2.5
HXYA-1A	1	49.2	5.9	18.62	15.58	38.72	0.993	0.70400	0.512850	4.1
HWGA-3	1	48.2	10.4	18.50	15.41	38.33	0.964	0.70357	0.512878	4.7
HXYB-5	1	49.3	7.6	18.59	15.56	38.72	0.996	0.70396	0.512838	3.9
HWPB0	1	52.3	7.3	18.54	15.45	38.44	0.971	0.70347	0.512872	4.6
HHJA-15	1	53.7	6.5	18.72	15.55	38.62	0.971	0.70386	0.512865	4.4
HLMA1-4	1	53.2	6.4	18.76	15.60	38.71	0.977	0.70337	0.512848	4.1
HWPA-12	1	53.6	7.1	18.58	15.48	38.42	0.965	0.70357	0.512884	4.8
HWPA-18	1	46.5	10.3					0.70311	0.512944	6.0
GD137	1	45.6	8.1	18.37	15.47	38.24	0.967	0.70336	0.512921	5.5
SY13-5	1	50.4	7.0	18.36	15.43	38.13	0.956	0.70320	0.512909	5.3
JY5	1	53.2	9.4	18.64	15.60	38.71	0.989	0.70363	0.512815	3.4
Y12-10	1	53.7	6.1	18.57	15.54	38.53	0.978	0.70326	0.512840	3.9
CK280	1	51.8	7.2	18.48	15.49	38.38	0.972	0.70368	0.512864	4.4
SY9-7	1	51.8	5.5	18.41	15.47	38.23	0.961	0.70318	0.512913	5.4
R8	1	50.0	8.1	18.62	15.56	38.82	1.004	0.70425	0.512791	3.0
AN6	1	50.9	8.1	18.62	15.56	38.55	0.975	0.70358	0.512844	4.0
GD9-10	1	52.4	9.6	18.60	15.55	38.48	0.969	0.70369	0.512893	5.0
T471	1	46.9	7.9	18.55	15.54	38.57	0.983	0.70325	0.512945	6.0
8-1	1	47.9	7.8	18.78	15.64	38.86	0.991	0.70415	0.512839	3.9
Hainan Island flood basalt										
HN9901	2	51.7	6.5	18.63	15.61	38.85	1.005	0.70385	0.512868	4.5
HN9902	2	50.8	6.8					0.70392	0.512884	4.8
HN9907	2	49.1	9.6	18.66	15.63	38.87	1.005	0.70418	0.512848	4.1
HN9908	2	45.3	10.3	18.69	15.65	38.88	1.002	0.70423	0.512869	4.5
HN9910	2	45.5	10.2	18.70	15.63	38.87	1.001	0.70427	0.512861	4.4
HN9912	2	45.3	10.3	18.71	15.62	38.85	0.998	0.70418	0.512862	4.4
HN1	3,4	48.6	9.1					0.70383	0.512891	5.0
HN10	3,4	50.8	6.9	18.73	15.60	38.84	0.994	0.70422	0.512876	4.7
HN19	3,4	48.8	5.4	18.62	15.60	38.82	1.003	0.70447	0.512859	4.3
HN22	3,4	49.6	6.5	18.46	15.61	38.88	1.027	0.70382	0.512866	4.5
HN27	3,4	47.0	9.0	18.66	15.61	38.87	1.004	0.70417	0.512874	4.6
HN33	3,4	49.4	7.5	18.65	15.61	38.89	1.008	0.70402	0.512885	4.9
HN36	3,4	52.5	6.3	18.67	15.60	38.85	1.002	0.70403	0.512871	4.6
HN40	3,4	51.8	6.5	18.68	15.62	38.91	1.006	0.70403	0.512907	5.3
HN41	3,4	52.1	7.1	18.72	15.65	38.98	1.010	0.70399	0.512819	3.6
HN55	3,4	49.1	7.9	18.67	15.61	38.98	1.015	0.70419	0.512868	4.5
HN62	3,4	47.5	8.4					0.70402	0.512912	5.4
HN76	3,4	50.5	6.9	18.64	15.58	38.79	0.998	0.70383	0.512930	5.7
HN77	3,4	50.0	7.1	18.66	15.61	38.88	1.006	0.70381	0.512926	5.7
HN83	3,4	51.5	7.2	18.59	15.54	38.69	0.992	0.70389	0.512925	5.6
HN90	3,4	52.4	7.3	18.68	15.57	38.78	0.993	0.70415	0.512908	5.3
HN91	3,4	52.2	6.8	18.74	15.61	38.90	0.999	0.70431	0.512881	4.8
HN95	3,4	51.7	6.9	18.67	15.62	38.99	1.017	0.70418	0.512866	4.5
HN97	3,4	46.9	9.1	18.65	15.54	38.71	0.989	0.70354	0.512876	4.7
HN98	3,4	46.9	8.1	18.62	15.52	38.67	0.987	0.70354	0.512897	5.1
HN99	3,4	46.9	8.0	18.62	15.51	38.64	0.985	0.70357	0.512881	4.8
Seamount basalt from the South China Sea										

V36D8-2	5	49.2	5.7	18.70	15.61	38.33	0.942	0.70359	0.512929	5.7
V32D8-4	5	49.7	6.1	18.60	15.63	38.85	1.009	0.70356	0.512916	5.4
V36D9-1	5	49.1	5.5	18.67	15.54	38.68	0.983	0.70443	0.512922	5.5
V36D9-2	5	48.9	3.4	18.95	15.59	38.99	0.986	0.70397	0.512813	3.4
V36D10	5	49.3	6.3	18.88	15.59	38.93	0.988	0.70401	0.512805	3.3
SO23-40	5	47.7	6.8	18.60	15.56	38.63	0.985	0.70381	0.512952	6.1
SO23-37-31	5	50.1	7.3	18.54	15.61	38.60	0.988	0.70399	0.512898	5.1
SO23-37-7	5	48.4	6.1	18.48	15.57	38.62	0.997	0.70394	0.512894	5.0
SO23-35-6	5	47.4	8.5	18.41	15.58	38.55	0.997	0.70436	0.512913	5.4
S04-11	6	44.8	7.8	18.69	15.60	38.83	0.997	0.70342	0.512965	6.4
S04-12-8	6	48.8	2.4	18.41	15.56	38.52	0.994	0.70396	0.512901	5.2
S04-12-12	6	45.4	3.8	18.62	15.60	38.77	0.998	0.70404	0.512863	4.4
S04-12-18	6	50.0	2.1	18.37	15.53	38.44	0.989	0.70396	0.512894	5.0
S04-12-20	6	47.0	5.9	18.50	15.60	38.67	1.000	0.70414	0.512855	4.3
S04-16	6	44.4	7.9	18.70	15.71	39.09	1.023	0.70366	0.512906	5.3
S05-34A	6	46.8	4.2	18.70	15.65	38.93	1.006	0.70377	0.512870	4.6
Late Cenozoic basalts from the Indochina peninsula										
NR-8	7	50.9	2.8	18.24	15.49	38.11	0.966	0.70384	0.512950	6.1
NR-9	7	50.8	3.6	18.28	15.51	38.19	0.971	0.70360	0.512947	6.1
NR-10	7	49.7	3.4	18.32	15.53	38.26	0.975	0.70380	0.512872	4.6
NR-11	7	47.5	5.9	18.23	15.49	38.17	0.975	0.70364	0.512956	6.2
NR-12	7	47.6	6.0	18.28	15.49	38.16	0.968	0.70382	0.512952	6.2
NR-13	7	47.7	4.9	18.26	15.52	38.23	0.977	0.70387	0.512957	6.3
PNG-33	7	43.5	6.8	18.30	15.48	38.21	0.972	0.70354	0.512906	5.3
PNG-34	7	43.6	6.5	18.32	15.48	38.22	0.971	0.70361	0.512897	5.1
PNG-35	7	48.2	4.8	18.47	15.53	38.41	0.975	0.70368	0.512865	4.5
BR-7	7	52.8	5.6	18.59	15.57	38.58	0.981	0.70550	0.512736	2.0
BR-17	7	49.5	6.6	18.49	15.54	38.48	0.981	0.70491	0.512787	2.9
BR-18	7	49.5	7.2	18.54	15.58	38.63	0.992	0.70486	0.512806	3.3
BR-19	7	50.9	6.0	18.52	15.54	38.67	0.998	0.70519	0.512747	2.2
PPK-6	7	53.0	5.5	18.58	15.56	38.55	0.978	0.70551	0.512714	1.5
PPK-20	7	51.8	3.7	18.65	15.60	38.72	0.989	0.70556	0.512689	1.0
PPK-22	7	52.6	5.5	18.66	15.54	38.51	0.966	0.70550	0.512697	1.2
PPK-23	7	49.9	7.0	18.51	15.53	38.43	0.973	0.70573	0.512685	1.0
PR-14	7	51.9	4.2	18.59	15.56	38.50	0.972	0.70581	0.512666	0.6
PR-15	7	52.3	4.2	18.56	15.56	38.55	0.981	0.70585	0.512659	0.4
PR-16	7	53.0	5.5	18.62	15.55	38.53	0.972	0.70579	0.512667	0.6
SR-25	7	53.6	5.2	18.65	15.57	38.60	0.977	0.70569	0.512681	0.9
SR-26	7	53.2	4.7	18.65	15.57	38.57	0.974	0.70570	0.512683	0.9
SR-27	7	52.6	6.0	18.64	15.56	38.84	1.003	0.70564	0.512706	1.4
OS-II	8	52.9	7.0	18.57	15.66	38.80	1.007	0.70402	0.512870	4.6
QN-3B	8	44.3	11.5	18.47	15.61	38.70	1.007	0.70403	0.512831	3.8
SC-5C	8	46.5	5.1	18.65	15.62	38.80	0.998	0.70496	0.512853	4.2
90/15	8	54.3	6.3	18.68	15.62	38.80	0.995	0.70585	0.512731	1.9
90/58	8	43.6	9.8	18.84	15.64	39.00	0.999	0.70450	0.512849	4.2
121/16	8	52.3	6.3	18.70	15.60	38.80	0.993	0.70512	0.512786	2.9
121/33	8	46.1	10.8	18.34	15.59	38.40	0.988	0.70414	0.512860	4.4
121/108	8	46.2	8.9	18.41	15.57	38.40	0.980	0.70434	0.512776	2.7
121/229	8	47.2	9.5	18.54	15.60	38.60	0.988	0.70483	0.512784	2.9
121/299	8	48.2	7.3	18.89	15.64	38.80	0.973	0.70497	0.512715	1.5
45/5	8	45.1	9.0	18.28	15.56	38.30	0.984	0.70393	0.512887	4.9
45/10	8	45.5	9.3	18.28	15.56	38.30	0.984	0.70385	0.512919	5.5
45/14	8	45.8	7.4	18.40	15.55	38.40	0.982		0.512919	5.5
45/17	8	47.4	5.5	18.41	15.56	38.40	0.980		0.512859	4.4
63/31	8	48.2	7.1	18.66	15.57	38.90	1.008	0.70383	0.512927	5.7
960/30	8	45.1	9.1	18.33	15.60	38.40	0.989	0.70394	0.512833	3.8
PL- 1	8	49.2	7.3	18.53	15.59	38.60	0.989	0.70392	0.512859	4.4
804/27	8	47.4	10.0	18.45	15.54	38.50	0.987	0.70383	0.512878	4.7

804/52	8	52.4	6.0	18.64	15.59	38.70	0.988	0.70356	0.512922	5.6
804/178	8	50.5	6.8	18.59	15.58	38.60	0.983	0.70377	0.512864	4.4
804/230	8	49.0	4.7	18.57	15.58	38.60	0.985	0.70429	0.512902	5.2
804/250	8	51.2	5.4	18.67	15.63	38.70	0.985	0.70396	0.512910	5.3
51 I/8	8	41.9	12.6	18.12	15.52	38.30	1.001	0.70412	0.512773	2.7
511/4	8	40.5	9.9	18.12	15.55	38.40	1.013	0.70416	0.512798	3.2
516/4	8	48.3	10.0	18.32	15.58	38.50	1.001	0.70428	0.512809	3.4
507/2	8	45.0	7.2	18.27	15.56	38.40	0.996	0.70435	0.512819	3.6
507/11	8	43.4	9.8	18.23	15.53	38.30	0.989	0.70431	0.512834	3.9
507/30	8	44.0	9.5	18.32	15.50	38.40	0.990	0.70435	0.512853	4.2
SL-I	8	57.6	3.2	18.24	15.59	38.50	1.010	0.70481	0.512716	1.6
R-2	8	50.0	5.6	18.19	15.54	38.30	0.993	0.70532	0.512708	1.4
756/4	8	52.9	6.2	18.71	15.61	38.80	0.992	0.70382	0.512813	3.5
736/24	8	51.3	7.1	18.45	15.54	38.50	0.987	0.70398	0.512882	4.8
736/240	8	51.2	6.7	18.62	15.59	38.70	0.991	0.70414	0.512824	3.7
9/85	8	47.2	8.4	18.78	15.64	39.10	1.016	0.70408	0.512819	3.6
CC-1	8	51.1	4.1	18.48	15.53	38.40	0.973	0.70356	0.513026	7.6

References (Ref.): 1-Han et al. (2009); 2-Zou and Fan (2010); 3-Major element (Flower et al., 1992); 4-Isotope (Tu et al., 1991); 5-Tu et al. (1992); 6-Yan et al. (2008); 7-Zhou and Mukasa (1997); 8-Hoang et al. (1996).

References

Flower, M.F.J., Zhang, M., Chen, C.-Y., Tu, K., Xie, G., 1992. Magmatism in the South China Basin : 2. Post-spreading Quaternary basalts from Hainan Island, south China. Chemical Geology 97, 65-87.

Han, J.W., Xiong, X.L., Zhu, Z.Y., 2009. Geochemistry of Late-Cenozoic basalts from Leiqiong area: The origin of EM2 and the contribution from sub-continental lithosphere mantle. Acta Petrologica Sinica 25, 3208-3220.

Hoang, N., Flower, M.F.J., Carlson, R.W., 1996. Major, trace element, and isotopic compositions of Vietnamese basalts: Interaction of hydrous EM1-rich asthenosphere with thinned Eurasian lithosphere. Geochimica et Cosmochimica Acta 60, 4329-4351.

Tu, K., Flower, M.F.J., Carlson, R.W., Xie, G., Chen, C.-Y., Zhang, M., 1992. Magmatism in the South China Basin: 1. Isotopic and trace-element evidence for an endogenous Dupal mantle component. Chemical Geology 97, 47-63.

Tu, K., Flower, M.F.J., Carlson, R.W., Zhang, M., Xie, G., 1991. Sr, Nd, and Pb isotopic compositions of Hainan basalts (south China): Implications for a subcontinental lithosphere Dupal source. Geology 19, 567-569.

Wang, X.-C., Li, Z.-X., Li, X.-H., Li, J., Liu, Y., Long, W.-G., Zhou, J.-B., Wang, F., 2012. Temperature, Pressure, and Composition of the Mantle Source Region of Late Cenozoic Basalts in Hainan Island, SE Asia: a Consequence of a Young Thermal Mantle Plume close to Subduction Zones? Journal of Petrology 53, 177-233.

Yan, Q., Shi, X., Wang, K., Bu, W., Xiao, L., 2008. Major element, trace element, and Sr, Nd and Pb isotope studies of Cenozoic basalts from the South China Sea. Science in China Series D: Earth Sciences 51, 550-566.

Zhou, P., Mukasa, S.B., 1997. Nd-Sr-Pb isotopic, and major- and trace-element geochemistry of Cenozoic lavas from the Khorat Plateau, Thailand: sources and petrogenesis. Chemical Geology 137, 175-193.

Zou, H., Fan, Q., 2010. U-Th isotopes in Hainan basalts: Implications for sub-asthenospheric origin of EM2 mantle endmember and the dynamics of melting beneath Hainan Island. Lithos 116, 145-152.